Master's Thesis

Feeding of Characteristic Modes in Multi-Antenna Handsets

Farnaz Chaman-Zadeh

Department of Electrical and Information Technology,
Faculty of Engineering, LTH, Lund University, November 2014.

Master's Thesis

Feeding of Characteristic Modes in Multi-Antenna Handsets

By

Farnaz Chaman-Zadeh

Department of Electrical and Information Technology
Faculty of Engineering, LTH, Lund University
SE-221 00 Lund, Sweden

Abstract

Multiple-input multiple-output (MIMO) antenna systems fundamentally require the radiation patterns of the antennas to be nearly orthogonal to one another. In a multipath environment, the orthogonality of the patterns allows for increased throughput, link reliability and coverage. The requirement of orthogonal antenna patterns is difficult to realize at low mobile frequency bands due to the small sizes of modern mobile handsets.

In this work, several MIMO terminal antennas operating at Long Term Evolution (LTE) bands below 1 GHz were analyzed using the Theory of Characteristic Modes (TCM). This analysis technique reveals all the characteristic modes and the corresponding orthogonal patterns that a structure is physically able to produce. Through the combination of the pattern of one or more modes, found through TCM analysis, any physically obtainable pattern can be produced. TCM is able to provide currents, near-fields, and far-fields for each orthogonal mode. These modal currents and fields were correlated to those of real antennas structures excited traditionally in CST simulation. The results provide valuable insight into the modes excited in many common modern mobile phone antennas and the underlying mechanisms for some antenna structures to outperform others of the same size and shape.

Acknowledgments

I would like to express my deepest gratitude to my advisor, thesis examiner, friends, and my family.

First and foremost I would like to express my gratitude and respect to my thesis examiner Associate Professor *Buon Kiong Lau* for the honor and privilege of performing my thesis project in his group, and for the opportunity to meet his group of motivated, inspiring young researcher.

I could never perform my thesis without the supervision of my advisor Ph.D. candidate *Zachary Miers.* His unlimited patience in answering my questions and his valuable comments are appreciated. I am grateful to him for his mentorship, sharing his knowledge and the unlimited assistance in all stages of performing my thesis.

I would like to thank my classmates and friends in the Master's Program in Wireless Communications, and the entire staff in the Department of Electrical and Information Technology (EIT), without whom the exceptional experience of staying in Lund would have not been the same.

Lastly I am grateful to my parents and my sister for their unconditional love, constant encouragement and support throughout my entire life. It was their understanding and reassurance that uplifted me when I got weary.

Table of Contents

CHAPTER 1

1 Introduction

1.1 Preface

Almost all recent wireless communication standards such as LTE, LTE-Advanced, IEEE 802.16 (WiMAX) and IEEE 802.11n emphasize utilization of multi-antenna techniques to meet the ever-increasing demand of high capacity services.

While the simple multi-antenna technique of diversity reception in the uplink is in widespread use throughout the world (e.g., in GSM systems), the deployment of MIMO techniques including spatial multiplexing in the downlink has remained a major challenge for designers of mobile devices [1]. One significant challenge lies in the limiting nature of a typical mobile chassis, whose small size makes it difficult to design antennas with orthogonal (or decoupled) radiation patterns [2]. The reason behind this difficulty is explained below through the Theory of Characteristic Modes (TCM).

TCM is a tool, which inherently describes the fundamental electromagnetic behavior of antennas at different frequencies. According to TCM, any structure is able to radiate a set of orthogonal modes. The total current distribution on the surface of the chassis for a given antenna feed excitation can be expressed as the superposition of a set of weighted orthogonal modal currents [3], [4]. The antenna feed contributes energy into different modes, distributing the current across separate characteristic modes.

In LTE bands below 1 GHz, the ground-plane of a standard smartphone typically has only one resonant mode. The single low frequency resonant mode of the ground-plane is typically called the fundamental mode. In a standard mobile handset, the fundamental mode often has the maximum electric near-field values along the short edges of the chassis. The E-field values decrease from the edges towards the center of the ground-plane, and reach the minimum value at the center. The fundamental mode generally has a dipole-like radiation pattern and a wider resonant bandwidth than other modes of operation. In order to excite a mobile antenna in the low band, a feed element will often couple into this fundamental mode. This allows for an acceptable resonant bandwidth. However, in the case of a multi-antenna system, if all the chassis feeds are coupled to this mode, there will be a significant amount of coupled power between the antenna elements. This coupling effect severely harms the MIMO performance. Selective placement of multiple feeds, as well as excitation of separate modes of operation, could reduce the aforementioned coupling between different elements [5].

To selectively excite specific characteristic modes, it is important to study the currents and fields of each mode individually. It is possible to choose the proper port location [5] and feeding technique [6] to isolate different modes of operation from coupling into one another. This guarantees significant improvement in system throughput and helps to achieve nearly orthogonal radiated patterns across the feeds.

Recently, it has been shown that TCM can be used in the process of designing electrically compact mobile antennas [7]. This has led to the development of several novel antenna systems which are capable of feeding separate modes of operation. Feeding separate modes effectively prevents one or more antennas from coupling into the fundamental chassis mode [8]. This method of designing MIMO antennas provides the resonant frequency and bandwidth of the excitable radiation modes of the entire structure without the introduction of an antenna feed [9].

On the other hand, each excitable mode, described by TCM, can also be used to analyze an implemented antenna structure. Thus, Characteristic Mode (CM) analysis provides information on possible methods to better optimize the antenna to increase bandwidth while decreasing antenna-to-antenna correlation.

1.2 Objectives

The goal of this Master's thesis is to investigate compact terminal MIMO antenna systems in relation to their fundamental characteristics through TCM. This is done by analyzing common MIMO terminal antennas, and relating these multi-antennas to the structures' characteristic resonances. This analysis shows how different port placements and feed types couple differently into separate characteristic modes. Through the analysis of the currents, near-fields, and far-fields of real antennas, the isolation between ports can be described by their theoretical characteristic modes.

In this thesis, four unique antenna prototypes were studied and simulated using both a traditional full-wave analysis technique, implemented in CST Microwave Studio, as well as CM analysis, which is based on the Method of Moments (MoM) impedance matrix. All four prototypes were simulated, and the results of the surface current distributions, near-fields and far-fields for both the full-wave analysis and the CM analysis were numerically compared to each other in Matlab.

An in-house Matlab program was used to calculate the modal currents and near-fields, whereas FEKO simulation was used to obtain the characteristic far-fields. The comparison between the full-wave simulation output and the characteristic modes yields information on the excited characteristic modes in each of the four antenna prototypes. Furthermore, the amount of energy going into each modal pattern in each feed is calculated through CM analysis.

Neither FEKO nor the in-house TCM code considered dielectrics in the calculation of characteristic modes (in the versions used for this thesis project). Hence, to have a valid comparison with the results of full-wave simulations, dielectric materials were removed from all the prototypes in the CST models. However, to understand the effects of dielectrics, they were added back to terminal prototypes in the far-field analysis in the last chapter of the thesis. This comparison is done to investigate the effect of dielectrics on the characteristic modes and on the energy absorbed into the different modes.

CHAPTER 2

2 Literature Review

In this chapter, the theoretical concepts of this thesis are studied. The following topics are presented and reviewed in this chapter: Multiple antenna systems, Theory of Characteristic Modes (TCM), feeding techniques, and similarity measures used in this thesis.

2.1 Multiple Antenna Systems

A multiple antenna configuration, with independent channels between the transmitting and receiving antennas, is essential for achieving additional diversity against fading and/or high spectral efficiency.

The independence of the channels can be achieved through using sufficient inter-antenna distance for antennas with the same polarization or through the use of cross-polarized antennas. When using co-polarized antennas, the element spacing requirements are 10 wavelengths (λ) for base-stations, and 0.5λ for mobile terminals. The difference in spacing requirement is due to the different angular spreads of the signal as seen by the base stations and mobile terminals [1]. For cross polarized antennas, low mutual coupling can be achieved when the antennas are relatively close to each other [1].

However, neither sufficient antenna spacing nor cross-polarization can be easily implemented in compact mobile terminals due to the small sizes of the chassis [2]. The challenge in forming orthogonal patterns on mobile terminals is discussed in detail in the following section.

2.2 Theory of Characteristic Modes

2.2.1 Literature

The Theory of Characteristic Modes (TCM) was first developed by Garbacz in an effort to predict the scattering behavior of arbitrary objects [4]. Later on, Harrington reconsidered the theory from a new perspective and refined it. This was valuable as it simplified the formulation in Garbacz' paper [3].

Initially, the theory considered only conducting bodies [3], [4], but later Harrington extended it to incorporate dielectrics as well [10]. The first applications of TCM were antenna shape synthesis and control of radar scattering [11], [12]. Recently, TCM has been used as a method to predict radiation fields of arbitrary conducting bodies (e.g., [13]). Thus, this theory has gained attention in antenna design as well.

Systematic design of antennas on a multi-antenna device by using different characteristic modes on a mobile chassis is helpful to achieve low mutual coupling, required by MIMO systems [13], [14], [15]. This is a key achievement when designing terminal multi-antennas in the frequency bands below 1 GHz, since the largest dimension of the mobile terminal is less than half a wavelength at these frequencies [2]. In these small systems, it is the chassis that operates as the main radiator in the low bands, rather than the antennas connected to it [16].

This point is used in [17] to locate the proper placement of antennas on the chassis in order to excite selective modes. This approach of designing compact MIMO antennas has been recently used to develop some novel chassis antennas [8], [9], [18]. The key idea of these designs is to optimize the antenna placement, and to increase isolation of the radiators mounted on the ground-plane by visualizing the modes that each antenna excites.

2.2.2 Introduction to TCM

TCM is a numerical technique based on the Method of Moments (MoM) calculations over an arbitrary body. Typically, characteristic modes are estimated in the absence of any excitations. This implies that the shape of the object is the only factor playing a role in the numerical calculations of different modes.

Characteristic modes provide a set of possible current distributions, changing over frequency [3]. Each distribution radiates specific fields in the near-field and far-field zones. The physical interpretation of characteristic modes is that they are represented by all the orthogonal far-field patterns that a body is able to radiate [3], [4]. Accordingly, proper excitation of separate modes by individual antennas leads to fully orthogonal patterns in the MIMO antenna system.

However, real antennas often contribute energy into a combination of multiple modes, with different amounts of energy coupled into each mode. For the low bands, each port mounted on a standard mobile chassis is typically able to excite up to two to three modes due to the limiting nature of the chassis in producing resonant modes in these bands [6]. Multiple modes are sometimes purposely excited to increase the resonant bandwidth, as was done in [9].

In TCM, the modal currents are calculated by solving the eigenvalue equation for characteristic impedance [4]

$$X(J_n) = \lambda_n R(J_n)\ , \tag{1}$$

where $R(J_n)$ and $X(J_n)$ are real part and imaginary parts of the characteristic impedance, respectively, J_n represent the eigencurrents (or eigenvector), and λ_n is the corresponding eigenvalue. Since both $X(J_n)$ and $R(J_n)$ are real, the estimated eigencurrents and eigenvalues are also real.

The impedance matrix is the key to finding the current distributions with zero mutual impedance, which results in orthogonal radiations. Each J_n is a unique current density. The total current distribution, on an arbitrary body, is determined by integrating all current densities over the surface of the object.

The eigenvectors represent the characteristic currents, whereas the eigenvalues are used to distinguish between the different modes at a given frequency. Through numerical calculations, eigenvalues are derived as functions of frequency in the range from -∞ to +∞. By following any given eigenvalue as it changes over frequency, it is possible to draw a corresponding figure for all eigenvalues. Figure 1 shows the eigenvalues or equivalently characteristic modes of a typical mobile handset chassis of dimensions 130 mm by 66 mm.

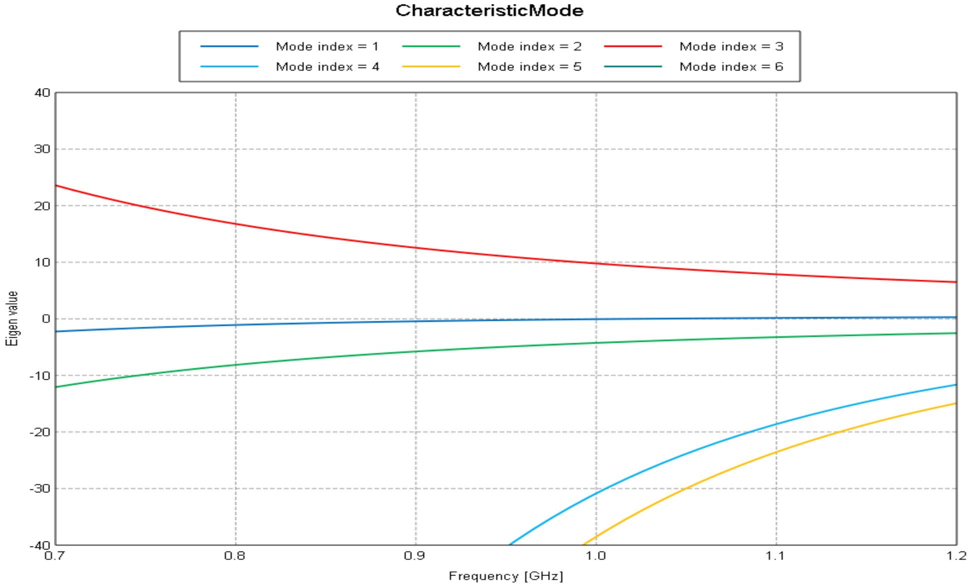

Figure 1: Eigenvalues of a standard handset chassis

According to the general resonant condition of a high frequency circuit, a system resonates at a given frequency when the imaginary part of its impedance is zero. The linear connection of resistance and reactance in the given eigenvalue equation, dictates that each mode resonates only when their related eigenvalue is equal to zero. As long as the eigenvalue in the figure remains zero, the imaginary part of the impedance is zero; meaning that the mode is resonant. Therefore, the resonant bandwidth of each mode relies on how the corresponding eigenvalue of that mode changes over frequency [5]. To paraphrase, the steeper the slope of the eigenvalue variations around zero, the narrower the resonant band of the corresponding mode.

In practice, eigenvalues close to zero (range of -15 to 15 in this thesis) are considered as modes that are excitable. These modes can be made to resonate if they are attached to an appropriate matching network.

Modes with positive eigenvalues are generally called inductive eigenmodes while those with negative eigenvalues are known as capacitive modes [3], [4]. Contrary to the inductive modes that store magnetic energy, the capacitive modes store electric energy [3]. The more the eigenvalues deviate from zero, the more difficult it is to couple energy into the corresponding modes.

In short, Figure 1 provides meaningful information about the resonant frequency of each mode, achievable bandwidth by exciting each mode properly, and the potential of exciting multiple modes at one frequency. It is clearly seen in Figure 1 that a standard mobile chassis (or ground plane) has only one resonant mode below 1 GHz. This mode is more or less the same for all small rectangular ground planes, including commercial modern mobile handsets with the largest dimension of approximately half a wavelength. This mode, known as the fundamental mode of the chassis [3], tends to have a relatively wide resonant bandwidth according to Figure 1. The majority of terminal antennas utilize this fundamental mode to yield wideband resonance. Consequently, the feeds mounted on the ground plane often dominantly excite this mode, which can lead to high correlation between different ports.

Figure 2 shows how slight modifications to the shape of a given structure changes the fundamental properties of the structure significantly. In this figure, the ground plane, as was described in Figure 1 was modified. Two identical inverted-F antennas (IFAs) were added to the short edges of the chassis. Adding the IFAs changed the characteristic modes of the chassis as shown in Figure 2. According to the figure, after adding the IFAs, more than one mode resonate below 1 GHz. Hence, this modified version has greater flexibility for diversity in designing terminal prototypes which are intended to excite separate modes. More details of this prototype are presented in Chapter 3.

Due to possibility of exciting only a few modes in the low band, the main contributors that are needed to fully describe the radiation behavior of a small body like a mobile phone are very few. In most physically compact chassis only a couple of modes are able to radiate energy. The reason behind this is that even modifying the ground plane and changing the eigenvalues can only enable two to three eigenvalues to resonate below 1 GHz. In other words, even by adding different parasitic elements to the chassis, there would not be more than two or three excitable modes below 1 GHz.

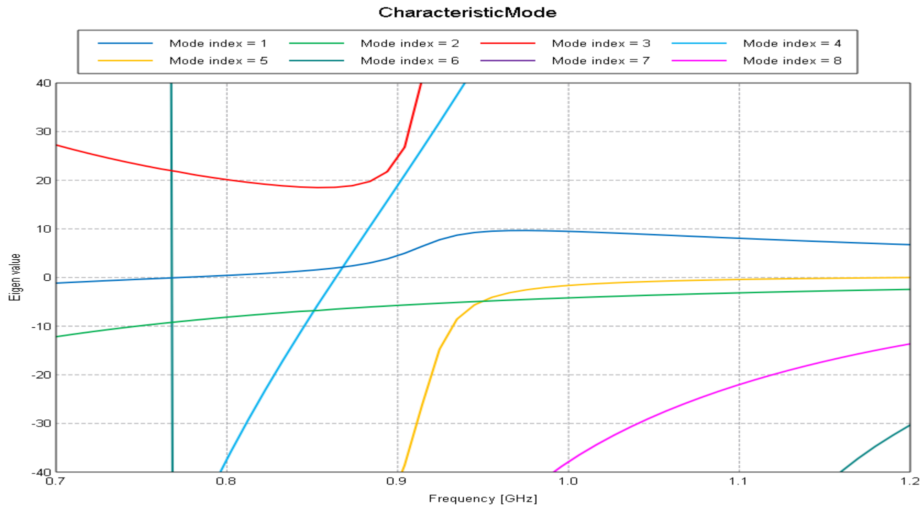

Figure 2: Eigenvalues of dual identical IFA

Likewise at a given frequency, modes with near zero eigenvalues can be excited more efficiently. Since it is very difficult to couple energy into other modes, they are not likely to be effectively excited in commercial prototypes. Therefore, this thesis focused on modes with eigenvalues deviating around zero at the operating frequency of the terminal prototypes.

In order to excite these modes, modal characteristics are used. Modal currents, and electric (E-) fields in the near-field zone are used to study the proper feeding method and port location. If proper mode excitation occurs, the excited current distributions will be roughly orthogonal. As a result, orthogonal patterns, which lead to the ideal MIMO performance, will be achieved.

2.3 Antenna Feed

In this thesis, the antenna feed refers to all components that are directly responsible for coupling energy into the structure. This definition covers capacitive coupling elements (CCE), inductive coupling elements (ICE) [9] and current feed elements, together with their matching networks. The antenna feeds are not directly responsible for the energy radiated into free space, but rather they match the antenna port to the free-space radiating element [19].

The characteristic mode impedance is solely dependent on the shape and size of the radiating structure. Since the chassis is the main radiator and determines the final impedance as seen by the port, the position of the feed on the chassis and the applied feeding techniques are of great importance in matching the port to the chassis. The impedance of the structure should be matched to the load impedance of the antenna in order to optimize the transferred power [20].

One solution of matching the port to the radiating structure through the antenna is to analyze the characteristic near-fields, which provide information on the locations where the magnetic and electric energy resides. With this information a designer can properly determine a suitable location to place a coupling element. A suitable point for exciting any of the arbitrary characteristic modes can be determined based on the near-field analysis of each mode. This technique also allows the designer to reduce the coupling between the feeds by determining the locations where the coupling elements will excite other modes (and hence avoid these locations).

The proper location of the feed on the chassis can be evaluated for some traditional simple antenna types through theoretical calculations. For instance, for a basic patch antenna, the location of feed can be estimated, theoretically, with acceptable approximations. However, in complicated designs, such as mobile phone handsets with multiple antennas or more complicated devices, special tools are needed to test the antenna performance while the feed is being moved along the surface of the chassis to determine the location with the optimum performance.

In order to transmit maximum power, a matching network between the transmission line and load is often required, regardless of the feeding method. In a mobile antenna design, moving the location of the feed and choosing feeding methods are useful tools in impedance matching. However, it is often useful to apply simple matching networks with several lumped elements, in order to increase the available bandwidth and power transferred to the radiating structure [21].

Lumped elements can reduce antenna efficiency, but proper feeding networks can greatly increase efficiency if properly implemented and designed. According to the small size of a mobile handset, the antenna element operates as the feed structure to the main radiator, which is the phone ground plane [22].

Using inductive and capacitive couplers is conventional to excite the chassis of small terminals. In these feeds, a non-resonant feeding strip couples energy through electric fields for the case of a CCE, or magnetic fields for the case of an ICE [20].

The location of the feed is also of great importance in exciting the desired modes. An arbitrary mode is excited inductively if an ICE is placed at the location of the maximum value in its current distribution. On the other hand, to excite a mode capacitively, a CCE must be placed at the location of its electric field peak [23].

Whereas inductive couplers are more effective than capacitive elements for exciting the desired modes without interacting with other modes [20], the capacitive feeds are useful in matching the antennas and obtaining an efficient MIMO system. Hence, correctly determining the feed topology is of great importance for increasing efficiency while maintaining maximum bandwidth.

As long as the coupling element remains electrically small, it does not have a significant impact on the total radiated energy [20]. As a result the entire structure will radiate the majority of the energy applied to the coupling element.

The profile appearance of the E-fields is important for optimizing feed position and excitation of selective modes because it shows how mounting a feed in a certain location induces fields on other sections of the chassis. This information helps to determine the best location for the second feed, based on the mode it tends to excite. This method of port placement is attracting interest in modern compact multi-antenna design, to eliminate the effect of high coupling on the ground plane caused by co-excitation of the chassis' fundamental mode [8].

Figure 3 shows an example of the fundamental mode's E-fields at a distance of 1.5 cm above the chassis. In many commercial single-antenna prototypes, the port is placed along a short edge of the chassis to excite this mode [24], [25], which often provides sufficient bandwidth for use within mobile frequency bands. Figure 3 indicates that placing a CCE on either the top or bottom short edge of the chassis excites this mode. Appendix 9.2 presents the fundamental mode of different prototypes, all of which have nearly similar E-fields near the ground plane, despite their many differences.

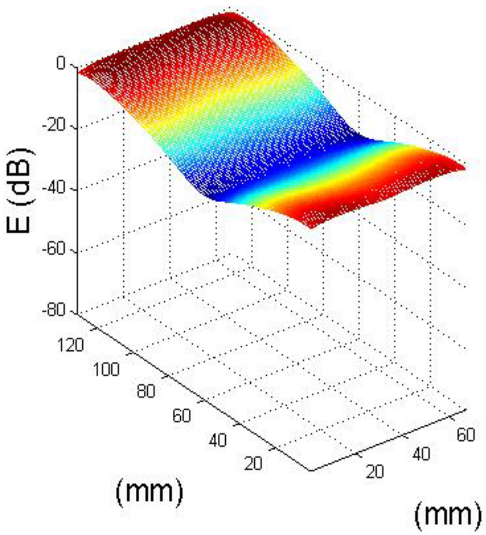

Figure 3: Fundamental mode's E-fields at 1.5 cm above the chassis

A single antenna feed can be used to couple energy into multiple characteristic modes, to either increase bandwidth or create multiband resonances. In [26], a coupling element is used to excite several different modes for both wideband and multiband operation. Figure 4 shows one of the antenna prototypes with capacitive feeds that was studied in this thesis. In this figure, one capacitive coupling to the chassis is provided by the monopole antenna, which is a dual band antenna with separate coupling strips for low band and high band operations [8].

When feeding a given mode of operation, either the electric or magnetic fields can be used. In this thesis, we study the coupling via E-fields due to the capacitive feeds that were used in all the studied prototypes.

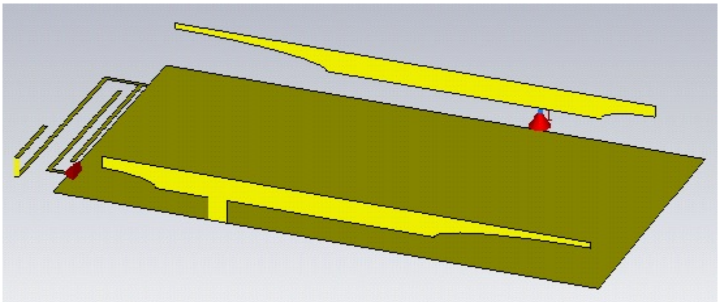

Figure 4: T-strip antenna prototype with capacitive feeds

2.4 Correlation Measures

This thesis investigates the participation factor of different characteristic modes in the overall radiation of an antenna port. In order to determine which mode is properly excited, to calculate the percentage of energy absorbed into each mode, and to understand how the final pattern is generated, the radiation properties of the characteristic modes are carefully compared to those of the actual antennas for the four antenna prototypes. The metrics used in this thesis to determine the similarity between the modal characteristics and the actual radiation characteristics of each prototype are summarized below.

2.4.1 Cross Correlation Coefficient

The cross correlation coefficient between two variables is a measure to indicate how the changes in one variable are related to the changes in a separate variable. This measure is used in pattern recognition to find the relation between two patterns or images. The total cross correlation between two matrices of the same size is estimated using 2D correlation. It is defined as [27]

$$CC = \frac{\sum\left(E_1 - mean(E_1)\right)\left(E_2 - mean(E_2)\right)^*}{\sqrt{\sum\left(E_1 - mean(E_1)\right)^2}\sqrt{\sum\left(E_2 - mean(E_2)\right)^2}} \quad , \qquad (2)$$

where the mean value is obtained by the equation

$$mean(E) = \frac{1}{m*n}\sum_{i=0}^{m-1}\sum_{j=0}^{n-1} E(i,j) \ . \qquad (3)$$

This measure is useful to determine the level of alignment between two related quantities, and used here in the current and E-field analysis to find the relation between the modal and actual antenna properties. This measure has the range of -1 to 1. If the value of CC is equal to 1, the two variables are fully correlated, whereas 0 and -1 indicate that there is no relation between the variables and the changes in the variables are not in the same directions, respectively.

2.4.2 Mutual Information

In information theory, mutual information is a measure to show how much information is accessible in one event by looking into another one. Mutual information is commonly applied in image processing alongside with correlation coefficient [27]. The results of both metrics are often compared to each other. In order to use this metric, it is necessary to align the pictures in a post processing procedure.

After the pictures are aligned, the joint histogram shows the joint event of the two different events. In this work, we use this metric to see how much information of each mode is available in the actual full-wave antenna parameter. The mutual information of two variables is given as

$$MI = \sum P(E_1, E_2).\log_2\left(\frac{P(E_1,E_2)}{P(E_1).P(E_2)}\right) \ , \tag{4}$$

where $P(E_1, E_2)$ is a 2D value of the joint event, calculated by using the joint histogram of the two normalized variables. $P(E_1)$ and $P(E_2)$ are the normalized values of the characteristic mode of interest and the CST output, respectively.

Normally, mutual information is not a normalized measure. Several different definitions were suggested in [27] and [28] to normalize it. In this work mutual information is normalized, using the self-information of each mode [27]. Self-information is all the information available in an event and it is defined as

$$I(E_1) = -\sum P(E_1).\log_2 P(E_1) \tag{5}$$

The Normalized Mutual Information (NMI) formula is [27]

$$NMI = \frac{(I(E_1)+I(E_2))}{(MI(E_1,E_2))} \tag{6}$$

2.4.3 Envelope Correlation Coefficient

Even though envelope correlation coefficient (ECC) is traditionally defined as the correlation between amplitudes (or signal envelopes), in this thesis it is defined as the square of the magnitude of complex correlation coefficient[1]. In this context, ECC is a metric for complex values, and it is widely used for quantifying spatial correlation in MIMO applications. ECC can be used to measure the orthogonality between two antenna patterns [19].

In this thesis, ECC is used to find how the antenna pattern is correlated to any given modal pattern. In other words, this measure gives the mode contribution in the final pattern in percentage. ECC follows the same form as Equation (2). The main difference is that the new function concerns both magnitude and phase values [29], whereas the previous measures only take advantage of the magnitude information.

Far-field analysis provides full pattern information and interprets the data in 3D spherical coordinates. Therefore, the information can be decomposed into the theta and phi polarizations. Using the magnitude and phase information in these polarizations, the contribution factor of each mode is estimated as [29]

$$|E_1|^2 = |E_{theta1}|^2 + \left|E_{phi1}\right|^2 \tag{7}$$

$$ECC = \frac{\sum(E_{theta1}.E^*{}_{theta2})\left(E_{phi1}.E^*{}_{phi2}\right).\sin(\theta_i)}{\sqrt{\sum(|E_1|^2.\sin(\theta_i))}\sqrt{\sum(|E_2|^2.\sin(\theta_i))}} \tag{8}$$

[1] It has been shown that ECC is approximately equal to the square of the magnitude of complex correlation.

CHAPTER 3

3 Mobile Antennas

This chapter gives a discussion of the four dual-antenna prototypes used in this thesis and a brief introduction of the location of each port. The prototypes shown are simulated without dielectrics.

3.1 Identical IFA Prototype

Based on [30], The IFA prototype includes two identical dual band IFA elements located on the top and bottom short edges of the chassis. Despite the fair efficiency and simplicity of this type of elements, IFAs have not been regularly in use for modern mobile phones, mainly because of its inherent narrow resonant bandwidth and high sensitivity to user interactions. The IFA elements are designed to capacitively couple energy into the chassis through a strip line feed element. The element is matched through a shorting stub. The two separate antenna feed points are mirrored along the length of the chassis with each feed attached to one of two short edges of the chassis.

The IFA elements will couple strongly to the fundamental mode of the chassis due to the capacitive feeding locations [5]. However, because of the offset of the feed from center of the short edge, some of the energy is coupled into other modes, which are orthogonal to the fundamental mode.

Under such a circumstance where the major portion of the power of both IFA elements is transferred into the fundamental mode, these elements are likely to experience very high correlation. This issue is discussed more in Chapters 5 and 6. Figure 5 illustrates the dual element IFA prototype. The feeds (enclosed in red spheres) can be seen on the two short edges.

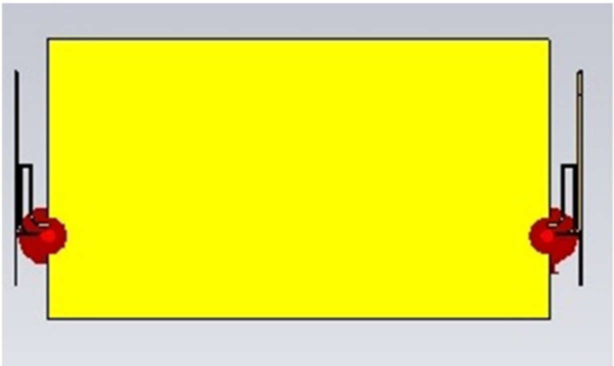

Figure 5: Dual band IFA Prototype

3.2 C-Fed Prototype

The dual band C-Fed (i.e. capacitively-fed) prototype consists of two mirrored meandering monopoles, located on the bottom short edge of the chassis [31]. Monopoles are meandered to reduce the occupied space by the antenna.

Both antenna elements couple energy into the chassis capacitively. Due to the mirrored structure, similar feeding strips are utilized for both elements. The two feeds are offset by 33 degrees from the chassis center and they are placed at the corners of the bottom short edge of the chassis.

Such a layout allows the capacitive feeds to excite multiple modes with E-field maxima along the short and long edges of the chassis. Consequently, the energy coupled to the chassis by these feeds is mainly from the first two low-order characteristic modes (see Chapter 5 and 6 for more details).

The antenna setup may result in a high correlation due to the feed position and capacitive feeding of the fundamental mode by both antenna elements. Chapter 5 discusses this aspect more and explains why the correlation between ports in the C-Fed (see Figure 6) prototype is less than the dual band IFA prototype.

The meandering antennas are implemented with dielectrics in the original version of the prototype, which affects the antenna performance. Figure 6 displays the C-Fed model in CST. The dielectrics are not shown in this figure.

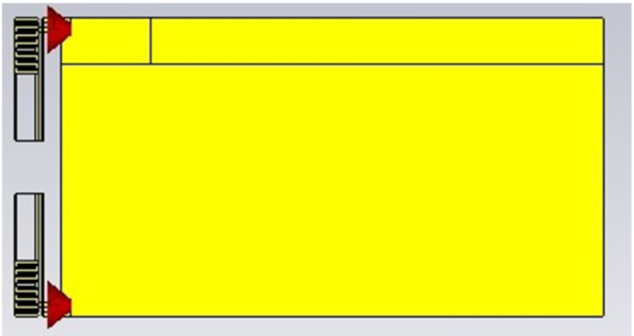

Figure 6: Dual Band C-Fed Prototype

3.3 PIFA-Monopole Prototype

Unlike the two previously introduced prototypes, the PIFA-Monopole prototype is not a symmetric structure. This multi-antenna structure has an improved overall MIMO performance because of the utilization of two different antenna types. The better performance may be explained by the lower mutual coupling between the elements of two different antennas.

Similar in principle to [32], this prototype has a planar IFA (PIFA), located at a corner of the bottom edge (see Figure 7), and a monopole located on the top short edge of the ground-plane (right side of Figure 7). The PIFA element in this prototype is an on-ground antenna, which is fed capacitively. Figure 7 illustrates the on ground-PIFA and the monopole in this prototype.

Figure 7: Dual-Band PIFA-Monopole Prototypes

The PIFA impedance is controlled by the feed line and shorting pin. This type of PIFA is simple to manufacture, but it resonates only in a very narrow band below 1 GHz [3]. The monopole is fed using a current feed, and has a lumped element attached to the feed to improve the resonance.

3.4 T-Strip Antenna Prototype

This prototype includes two different types of dual band antennas [9]. A monopole, placed on a short edge, and two T-strips, mounted on the longer edges of the chassis, form this prototype (see Figure 8).

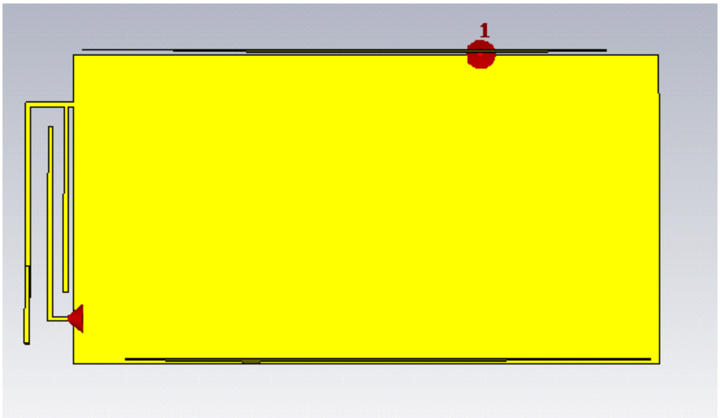

Figure 8: T-strip antenna Prototype

The monopole provides good bandwidth. The bandwidth of the T-strip antenna is controlled by the excitation of selective characteristic modes [9]. This prototype was designed based on characteristic modes; therefore, the coupling between the MIMO elements is very low.

Monopole antenna is fed capacitively, whereas the connecting pin between the T strip and the ground plane is a current feed. This strip loads the T strip (Figure 8) on the other long edge of the ground plane capacitively. The size of the shorting pin between the T-antenna and the chassis is used to tune the resonant frequency.

There is an almost 90 degrees offset between the feeds, which allow the antennas to couple energy into the chassis in separate modes. The monopole mainly excites the fundamental mode whereas in the T-Strip the second order mode is excited to be the dominant mode. Exciting different modes results in nearly orthogonal patterns [9]. (More details are given in Chapters 5 and 6.)

CHAPTER 4

4 Simulation Setups

This chapter talks about different computer programs used in this thesis work. The initial setups required by each program before simulating each prototype are briefly discussed. More detailed settings are presented in the following chapters when they are needed for specific analyses.

4.1 Matlab

Characteristic modes of the studied structures were obtained using an in-house Matlab program. The program is able to calculate different characteristic parameters, such as characteristic impedance, eigenvalues, characteristic current distributions, modal near-fields and modal far-fields of the antenna. This software estimates the characteristic modes for conducting bodies and neglects the dielectrics used in the structure to keep the calculations simple.

The program applies MoM on the Electric Field Integral Equation (EFIE) to calculate the current distribution as the basic characteristic parameter on the surface of the chassis. For this purpose, the metal object was divided into triangular grids using RWG (Rao-Wilton-Glisson) edge elements. An edge element consists of a couple of neighboring triangles with a common edge [33]. The MoM impedance matrix was calculated for each edge element. Hence, the number of elements in the impedance matrix is the same as the total number of edge elements.

Given an impedance matrix, Equation 1 in Section 2.2.2 was applied to obtain the eigenvalues and the corresponding eigenvectors. The eigenvalues were evaluated at a chosen frequency band. For this work, the band of operation was chosen as the operating frequency of the designed mobile terminals (824 to 894 MHz). The eigenvalues were calculated and plotted for each of the four terminal antenna prototypes, which allowed for the determination of the resonant characteristic modes at the frequency band of interest. The eigenvalue figures for each terminal prototype can be seen in in Appendix 9.1. According to these figures, the near resonant modes that are feasible for the coupling of energy were selected for further analysis. The reason that a frequency band below 1 GHz was chosen in this thesis is to simplify the analysis to only a few near resonant modes and to gain insight into the difficulty of forming orthogonal antenna patterns in the low band.

Using the CM program, the surface current distribution of each selected mode was calculated in Matlab by integrating current density of all grids over the surface of the chassis. The total current distribution of the chosen mode can then be plotted over the surface of the chassis. Carrying out the same procedure for different modes offers a set of orthogonal real currents on the chassis in the frequency band of interest.

Once the desired characteristic current distribution of a given chassis (together with its antenna elements) was calculated, the electric and magnetic fields of that mode were estimated in the near-field and far-field zones of that prototype. The distance above the ground plane for calculating the near-fields is adjustable in the program and it was set to 15 mm in this thesis. To estimate the near-fields, the plate was divided into small dipoles. The fields over the chassis were calculated as the sum of radiated fields by individual dipoles over the chassis. The estimated near-fields do not include the phase information. This aspect will be discussed in greater detail in Chapter 6.

The far-fields for each structure were calculated at the distance of 100 meters from the chassis. Then, the radiated fields were normalized to a distance of 1 meter from the object. This research analyzed the electric fields, and not the magnetic fields, due to the majority of the prototypes relying on capacitive coupling elements for excitation.

4.2 CST

Full-wave simulations were carried out on each antenna prototype, in an effort to understand the properties of each chassis once the antennas were properly tuned and implemented. The full wave simulations were performed in CST Microwave Studio using the finite element solver. The results were correlated to the characteristic modes, which were solved using Matlab.

For a valid comparison between the output of CST and the characteristic modes solved in Matlab, all models were setup in both programs to work with one another. As discussed, for simplicity the dielectrics were removed when solving each chassis using the TCM. This same condition was applied to the full wave models in CST in order to have a valid comparison between the results. Removing the dielectrics from all prototypes allows the current distribution and resonant frequency to remain constant between different simulation techniques. Figure 9(a) shows a PIFA–Monopole antenna with dielectric. The prototype without dielectrics is shown in Figure 9(b).

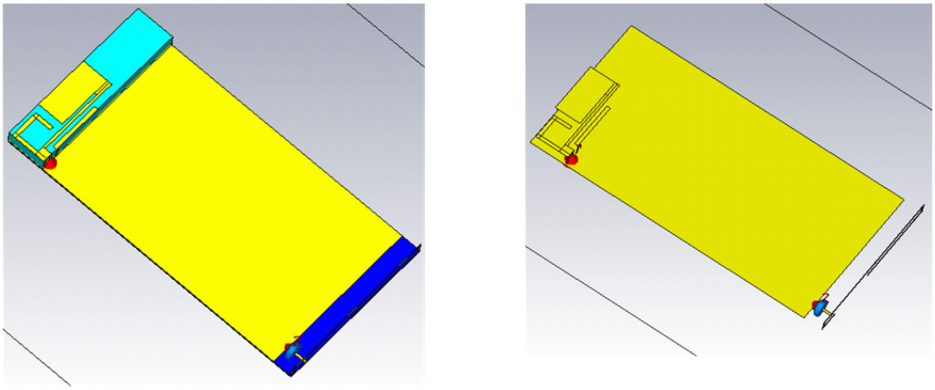

(b)

(a)

Figure 9: PIFA-monopole prototypes (a) with dielectrics (b) without dielectrics

Dielectrics are often used in terminal antennas as support structures for the antenna elements, as well as to support multi-layered PCB manufacturing. This not only makes the chassis physically stronger, but also allows for greater complexity to be introduced into the mobile terminal due to their (higher than free-space) permittivity. Dielectrics have many effects on antennas including, but not limited to, increased concentration of physical currents and fields, as well as reduction in wavelength. Dielectrics were neglected in this research to reduce the total complexity of the calculations and to allow for a more simplistic and theoretically robust analysis using TCM. Wavelength inside the dielectric is calculated as [35]

$$\lambda_{antenna} = \frac{\lambda_0}{\sqrt{\varepsilon_r}} \quad , \tag{9}$$

where $\lambda_{antenna}$ is the wavelength inside the dielectrics, λ_0 is the wavelength in free space and ε_r is the dielectric constant. This equation describes why dielectrics allow for more compact antennas to have the same resonant frequency as larger antennas which do not utilize dielectric materials. Removing the dielectrics without changing the physical shape of the structure will often increase the resonant frequency. It is not possible to maintain the identical characteristics of the antenna with the dielectrics removed. In order to maintain the same resonant frequency, a matching network is required after removing the dielectrics [34].

Dielectrics do not significantly impact the resonant frequency of the dual band identical IFAs, PIFA-Monopole, and T-Strip antenna in the low resonant bands of operation; therefore, it was deemed acceptable to utilize these antennas without dielectrics for this analysis. Figures 10 and 11 show the scattering (S) parameter of the identical IFAs with and without dielectrics, respectively. As expected, the resonant frequency is slightly higher after removing dielectrics.

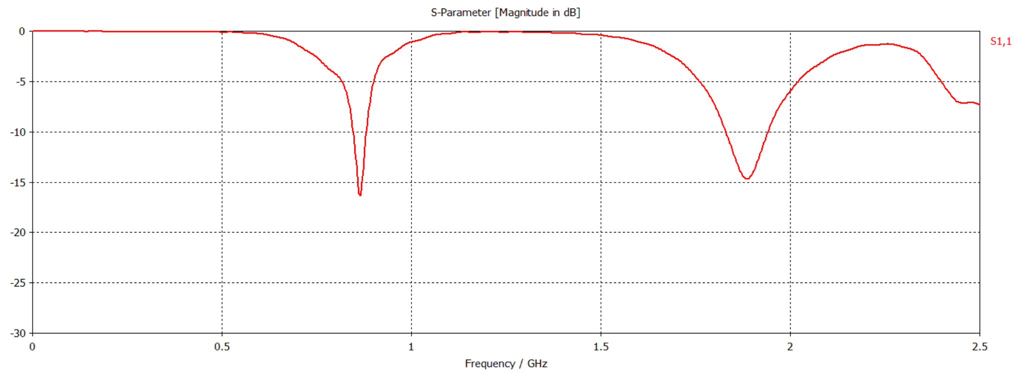

Figure 10: IFA with dielectrics

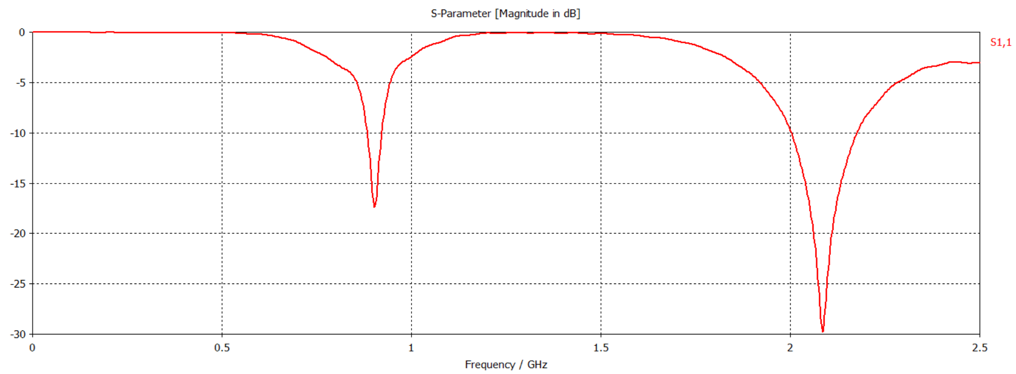

Figure 11: IFA without dielectrics

The C-Fed antenna is a more complex antenna, which heavily relies on the fields within the dielectric material. The C-Fed is shown with and without dielectrics in Figure 12. The dielectrics cover the arms of each antenna (left figure), which are used to match the antenna elements. Removing these dielectrics significantly impacts the performance of this type of feed.

When the dielectrics are removed, the antenna prototype is no longer resonant in the band of interest. In an effort to evaluate the basic characteristics of this chassis, the structure of the prototype was left untouched after the dielectrics were removed. In order to match the C-Fed in the band of interest, lumped elements were used in CST, which allowed the antenna to become resonant. However, removing the dielectric material may have significantly impacted the fundamental physics behind this antenna. The lumped elements allowed the C-Fed, which originally had a wide resonant bandwidth, to become resonant in a very narrow band without dielectrics. Figures 13 and 14 show the S parameter of the C-Fed with dielectrics, and tuned after removing the dielectrics, respectively. All prototypes were simulated in both programs, and the surface currents, near-fields, and far-field results were stored for the frequency 884 MHz.

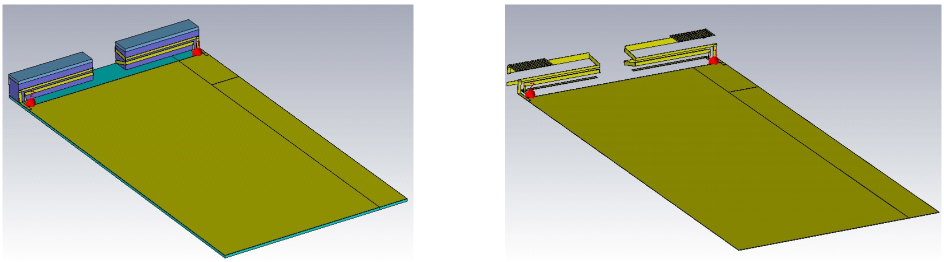

(a) (b)

Figure 12: C-Fed (a) With Dielectrics (b) Without Dielectrics

The far-field E-field patterns were calculated over the full sphere in step sizes of 5° in the theta plane and 5° in the phi plane. CST uses near-field to far-field transformations to calculate the far-field pattern, therefore CST requires a distance from the object being solved. In CST, this distance is set to 1 meter by default. However, for this research the fields were set to be solved at a distance of 100 m in CST. Characteristic fields are also calculated at 100 m to have a valid comparison between the actual antenna fields and the modal fields.

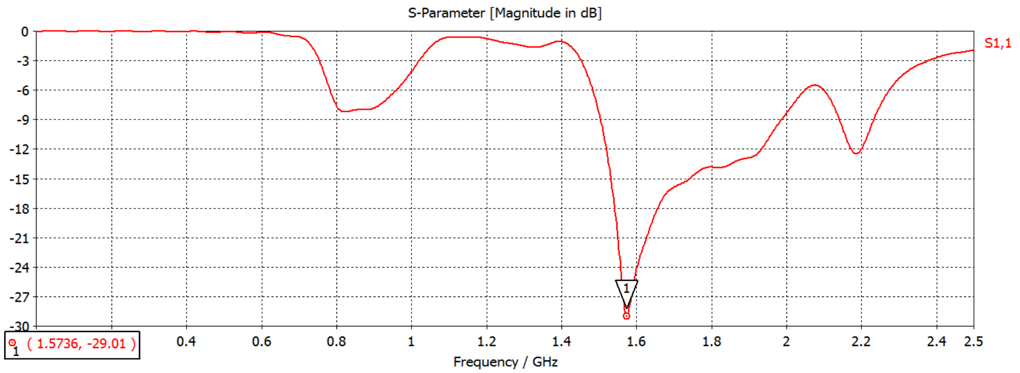

Figure 13: C-fed with dielectric

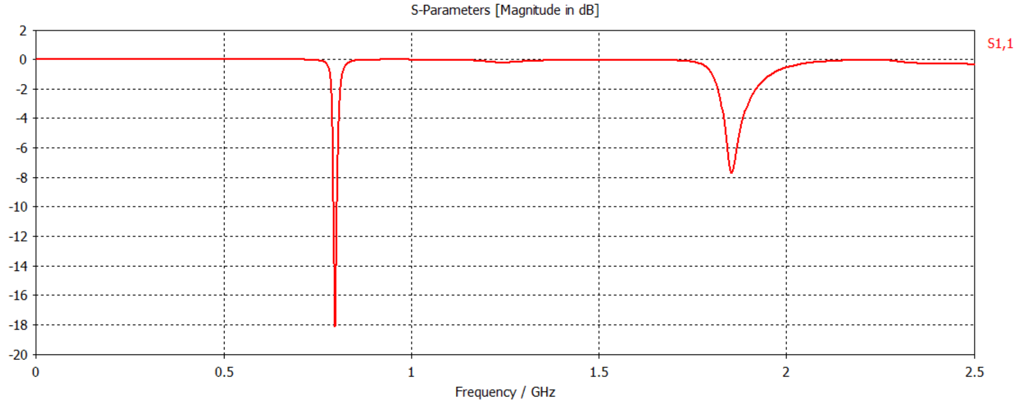

Figure 14: C-Fed re-tuned without dielectrics

4.3 FEKO

The far-field patterns of characteristic modes were computed in both Matlab and EMSS FEKO. For simplicity, the FEKO results were used when analyzing the far-fields between CST and TCM. The far-fields in EMSS FEKO were estimated in 3D spherical space. In the version used for this project, FEKO did not consider the dielectrics in the characteristic mode solver. Each prototype was simulated, and modal fields were exported at the resonant frequency for the first 6 low order modes. The modal fields were correlated to the actual fields that were solved for the terminal prototypes without dielectrics in CST. For simplicity, the same theta and phi step sizes as were applied in CST were used in the FEKO simulations.

CHAPTER 5

5 Current Distribution

In this chapter, the performances of the four different prototypes are investigated according to the feeds and the current distribution on the chassis. The excited modes of each prototype antenna are realized based on the modal current distributions, the location of the feed and the applied feeding method.

5.1 Post Processing in Matlab

After applying the general setup in Chapter 4 to each program, the modal currents and simulated current distributions were estimated and stored. The current simulation results in the two programs were carefully matched in a post-processing stage before a detailed comparison could be made between them. This section explains this post-processing stage in detail.

In this thesis, the modal currents were calculated using an in-house MoM program. To simplify the analysis, only the current distributions of potential excited modes near the full-wave resonant frequency are analyzed. The corresponding modes are the modes with eigenvalues in the range of -15 to 15 in the resonant band of the antenna as was explained in Section 2.2.

The excited current distribution on the chassis was obtained through a full-wave simulation in CST at frequencies near the resonance. The results of each simulation were stored and transferred to the characteristic modes program for further analysis.

The CST and the Matlab TCM programs apply different segmentation techniques in solving for the currents on the structure. The structures' currents in the TCM program are sub-divided into individual non-overlapping triangles. This is different than how the currents are sub-divided in CST, which uses hexahedral current grids.

The full-wave simulated currents were exported to Matlab. Although the CST model mesh is discretized through an adaptive mesh algorithm with high precision, the software does not give access to the discretization points. Hence, the mesh discretization is unknown in the CST model when the currents are exported. Hence, inevitably the transferred data from CST is matched to the available meshing in the TCM program rather than matching the TCM results to the CST mesh.

For this purpose, all information provided about the coordinates of each exported current point in CST is used. The exported information from CST is the average current on each divided section of the chassis, the coordinates of the central point of the grid, and the area of that sub-division. The problem of addressing the mismatch between the two separate meshes was solved through transferring the center point of each grid from CST and mapping each center point to individual triangles in the TCM mesh. The following post-processing steps were followed to find the corresponding TCM triangle for each of the CST currents.

1. Before saving the full-wave results, the local coordinate systems of both the TCM and the CST models were manually checked to verify compatibility, which simplified the post-processing procedure. Hence, X, Y and Z directions were aligned between the two programs.
2. The misalignment problem between the coordinate systems was then solved by transferring the center of one system to that of the other one.
3. TCM mesh grids were used to plot the CST simulation results in Matlab. Due to the more precise grids in CST, in contrast to the coarser grid used in the TCM analysis, there were multiple CST points that lied in each RWG triangle element. In order to find all the points located in each triangle element, the vectors between an arbitrary point in CST and all three vertexes of each triangle element in TCM were estimated. The magnitudes and directions of each set of triple vectors were stored in Matlab. The direction of each vector was displayed by an angle

value, which was used to check the location of the point. If the superposition of the three angles in each set was equal to 360 degrees, then the point was located inside the corresponding triangle element.

4. The CST currents were exported in complex form while the characteristic currents were exported as real currents [3], [4]. Due to this difference the imaginary parts of the CST currents were eliminated[2].
5. Each triangle element in the TCM program contains multiple CST exported points. The actual current value of that grid is calculated by averaging the currents of all the CST points located inside that element.

Figure 15(a) shows the current distribution of the dual identical IFA prototype in CST, and Figure 15(b) displays the same currents when they were transferred, and plotted using the TCM mesh grids in Matlab. It can be seen that the CST currents were smoothed and interpolated upon the transfer. The different segmentation between the two programs had affected the accuracy of the results, but the overall behavior of the current distribution remained unchanged. This provided enough evidence to support a study of the current distribution, based on the currents obtained by the two different programs.

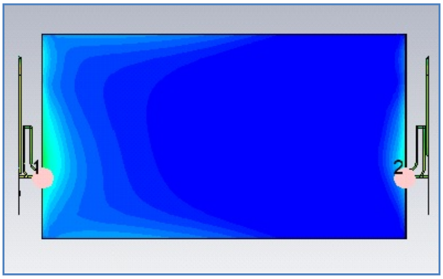

(a)

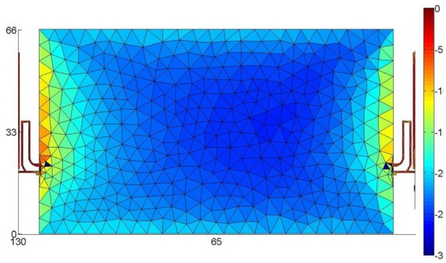

(b)

Figure 15: IFA simulated current distributions in (a) CST and (b) triangular mesh of Matlab

---

[2] It was discovered during the thesis review process that the magnitudes of the currents, and not only the real parts, should have been used instead. Accordingly, the conclusion in this thesis about the effectiveness of current correlation may change if this inaccuracy is revised.

5.2 Analysis of Current Distribution

As explained in Chapter 2, characteristic currents were the first characteristic property to be calculated in TCM. After the current distributions were successfully transferred to Matlab through use of the modal currents, it was possible to study appropriate locations to excite the characteristic modes selectively. This section investigates the excited modes based on the modal current distributions and the feed properties. The actual current distributions were studied in order to find out how the combination of several modes affected the final current flow on the chassis. In this section, the first resonant mode is referred to as λ_1. Higher order modes are called λ_2, λ_3, and λ_4.

5.2.1 Identical IFA Prototype

The excited CST currents at both ports, for identical IFA prototype, were plotted in Matlab. Figures 16(a) and 16(b) show the CST current distributions of one port while the other port is not excited (i.e., terminated in 50 ohm). Because the structure is completely symmetrical, the currents produced with port 1 excited are symmetrical to the currents with port 2 excited. In both figures, the current values are stronger along the short edges where the IFA elements were added to the chassis.

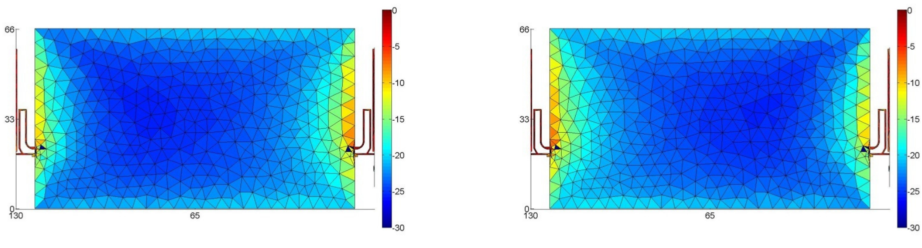

(a) (b)

Figure 16: CST IFA current distributions with (a) port 1 excited and (b) port 2 excited

A glance at of the actual current distributions (Figure 16) shows that exciting one port induces significant currents on the non-excited port. Moreover, the feeding arm was connected to a point with a very low current value, which is shown in the figure with a dark blue triangle on the chassis.

According to the capacitive type feed, this port was appropriately located to feed the antenna.

After the investigation of the actual current distributions, the characteristic current distributions were analyzed to find the excited modes by each port connected to the identical IFA prototype. The characteristic currents of the four modes closest to resonances were studied because other modes were unlikely to be excited. The current distributions of all these modes are presented in Appendix 9.2.

A comparison between the actual currents (Figure 16) and the characteristic currents of the different modes reveals that the current distributions of both ports have the highest correlation to the fundamental mode. Figure 17 shows the current distribution of λ_1, which has high current values along the edges of the chassis.

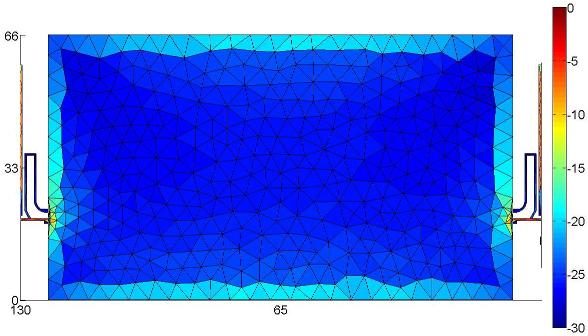

Figure 17: Characteristic current distribution of the fundamental mode for identical IFA prototype

The characteristic current distribution of the fundamental mode suggests placing a capacitive feed at the short edges of the chassis excites λ_1 strongly. In this particular IFA setup, the coupling performance is affected by both elements co-exciting the fundamental mode. In addition, the current overlap from one port on the other one is significant.

Both IFA ports were offset from the center of the short edge. Consequently, they were able to excite other modes as well, but none as strong as λ_1. Since the prototype is fully symmetric, it is expected that port 1 and port 2 excite same modes with similar participation factors. This leads to the two ports radiating approximately the same fields through the chassis. In other words, port 1 and port 2 produce almost the same current flow on the chassis; therefore, the final radiation patterns of the two different antennas are far from being perpendicular and are correlated significantly.

In Tables 1 and 2, similarity measures in terms of current correlation and normalized mutual information (NMI) between the first fours modes and port 1 on the chassis are shown. The calculated factors between these modes and port 2 are the same, since the structure is fully symmetric. However, utilizing this method of correlating the currents does not provide accurate weighting factors for the different modes. Hence, it does not allow accurate information on which modes are excited more or less than the other modes.

Table 1: Current correlation for identical IFA prototype

Correlation	Port 1
λ_1	0.54
λ_2	0.55
λ_3	0.56
λ_4	0.44

Table 2: NMI for identical IFA prototype

NMI	Port 1
λ_1	0.32
λ_2	0.33
λ_3	0.33
λ_4	0.25

5.2.2 C-Fed Prototype

The CST current distribution on the C-Fed prototype produced by the two ports are shown in Figures 18(a) and 18(b), respectively. As shown, the currents have mirrored distributions due to the inherent symmetry along the width of the chassis.

The current distributions in this prototype can be seen to have a diagonal trend. Due to this distribution, it was not possible to determine the dominant excited mode through visual comparison between the actual currents in CST and the modal currents in TCM directly; meaning that there is more than one strongly excited mode, which could be recognized by analyzing the characteristic currents.

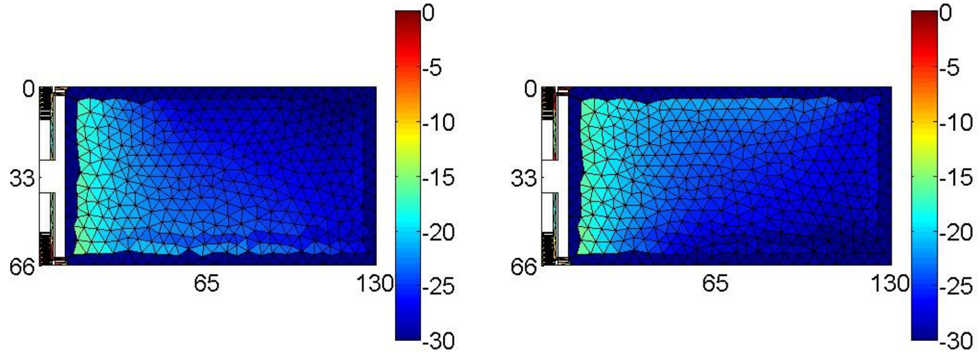

(a) (b)

Figure 18: CST C-Fed current distribution with (a) port 1 excited and (b) port 2 excited

Knowing that both antennas were fed capacitively, excited modes are found here according to the location of the ports (i.e. checking the current passing through the ports for a given mode). Figures 19(a) and 19(b) show modal currents of the first two resonant modes. In this figure, the first mode is distributed vertically (i.e., along the length) while the second mode is distributed horizontally (i.e., along the width). These two modes have strong currents in the corners of the chassis, where the capacitive feeds were located. Therefore, these feeds excite both $\lambda_1$and λ_2 dominantly. This result is similar to what was achieved in [20]. As this description clarifies, the current distribution in Figure 18 is achieved through the summation of these two modes and the co-excitation of the vertical and horizontal modes led to the diagonal current distribution.

According to the mirrored 33 degrees offset of the feeds from the center, both feeds excite the same modes with identical contribution factors. The current overlap from one port on the other one is shown in Figures 18(a) and 18(b). This overlap is not as severe as the port overlap in the dual identical IFA prototype, as will be explained below.

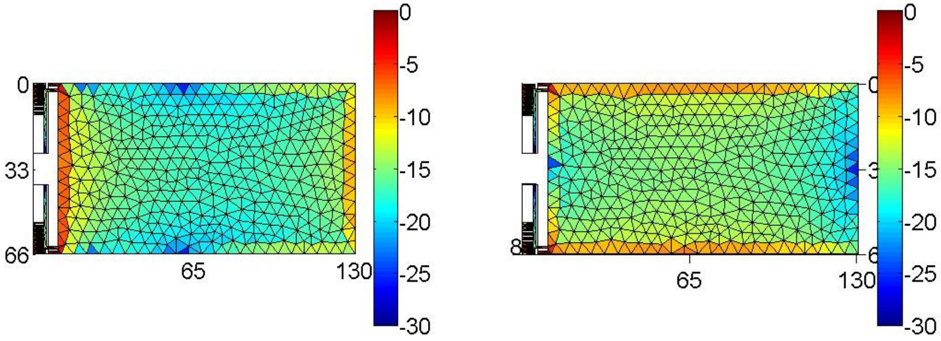

(a) (b)

Figure 19: C-Fed characteristic current distribution for (a) mode 1 and (b) mode 2

The two C-Fed antenna ports force the currents to flow diagonally across the chassis, but along two separate diagonals. In a square chassis, this would cause the two antennas to have perpendicular current distributions that allow for orthogonal currents to form. However, on the handset chassis, the current flows are not perpendicular due to the rectangular ground plane. Thus, the elements are not fully de-correlated. The total performance in the C-Fed prototype is significantly better than that of the mirrored identical IFA prototype as more than one dominant mode is excited and the energy is split between the different modes of operation.

Tables 3 and 4 contain the current correlation and NMI between port 1 antenna and the first four modes. It is seen that, as with the IFA prototype, it is not possible to find which modes are more excited than the others according to correlation measures used in this thesis.

Table 3: C-Fed current correlation

Correlation	Ant1
λ_1	0.49
λ_2	0.48
λ_3	0.47
λ_4	0.56

Table 4: C-Fed NMI

NMI	Ant1
λ_1	0.25
λ_2	0.3
λ_3	0.25
λ_4	0.3

5.2.3 PIFA-Monopole Prototype

For the PIFA-monopole prototype, Figures 20(a) and 20(b) present the simulated current distributions of the monopole and PIFA, respectively. According to the figure, the monopole currents are distributed along the chassis, whereas the PIFA has a more localized current distribution.

The monopole is a different type of capacitively coupled element than previously examined elements. The characteristic currents are analyzed to find the excited modes. The current distributions of the four studied modes are presented in Appendix 9.2. The characteristic currents show that the fundamental mode (Figure 21) has a very high correlation to the actual current distribution on the chassis of the monopole (Figure 20(a)).

Moreover, this mode has high current value where the feed is located. Therefore, the current feed excites this mode strongly. The current distributions of other modes, shown in Appendix 9.2, also suggest the excitation of λ_4 through this type of feed. However, based on the eigenvalues of the characteristic modes (see Appendix 9.1), coupling into this mode is more difficult than coupling into the fundamental mode.

The current distribution of the PIFA (Figure 20(b)) indicates that the PIFA is also fundamentally feeding substantial currents into λ_1. The fundamental mode, which is the dominant mode excited by the PIFA as well as the monopole, induces currents on the other side of chassis where the monopole is located. However, the current overlap from the PIFA to the monopole is reduced by the current localization of the PIFA [21].

As was seen in the previous sections, the fundamental mode is generally the main component in the radiation due to the ease of exciting this mode. Higher order modes have narrower bandwidths, which may be used as secondary modes to enhance the resonant bandwidth. In order to achieve acceptable bandwidth, either the wideband fundamental mode can be used as the dominant mode or a group of narrowband modes can be jointly excited to enhance the resonant band [9]. These higher order modes are not always the dominant modes.

Unlike the previous prototypes, this structure is not symmetric as it uses two different types of elements. Therefore, the total power contributions to each mode for port 1 and port 2 are different. This allows for the possibility of improving the isolation of the radiated fields as compared to the IFA prototype.

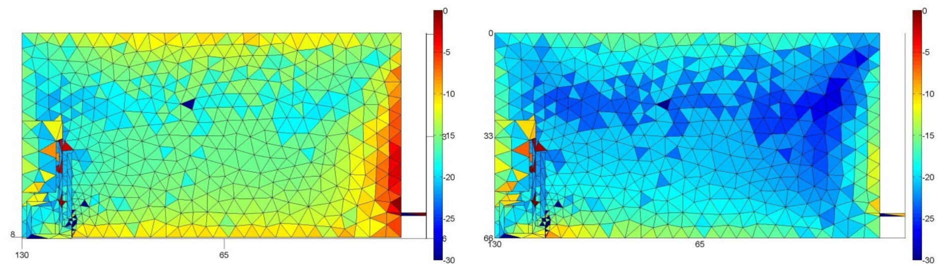

(a) (b)

Figure 20: CST current distribution with (a) monopole excited and (b) PIFA excited

Table 5: PIFA-monopole current correlation

Correlation	PIFA	Monopole
λ_1	0.11	0.32
λ_2	0.323	0.17
λ_4	0.10	0.29
λ_5	0.18	0.04

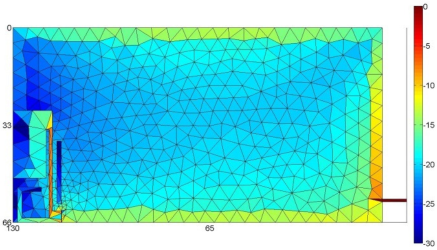

Figure 21: Characteristic current distribution of the fundamental mode

Table 6: PIFA-monopole NMI

NMI	PIFA	Monopole
λ_1	0.09	0.21
λ_2	0.12	0.08
λ_4	0.07	0.22
λ_5	0.14	0.14

5.2.4 T-Strip Antenna Prototype

The T-strip-monopole antenna was simulated in CST and the simulated current distributions of the monopole and T-antenna are shown in Figures 22(a) and 22(b), respectively. The monopole is located on the short edge, and its currents are strongest along this edge (Figure 22(a)). This current distribution is highly correlated to that of the fundamental mode of the chassis (with the antenna elements included), meaning that monopole transfers energy into the fundamental mode more than any other modes. The current distribution of the fundamental mode is presented in Appendix 9.2.

The T-antenna (see Figure 22(b)) shows a high correlation to λ_2 in current distribution. Mode λ_2, similar to the T-antenna, has high current values along the longer edges of the chassis, which illustrates the excitation of λ_2 by the T-antenna. However, λ_2 is not the only mode with high currents along the longer edges. The current is also high on the long edges in λ_4 (Appendix 9.2). Due to the current feeding of the T-antenna, this antenna is exciting λ_4 as well. But λ_2 is excited more than λ_4, due to stronger excitation of lower order modes.

According to Figure 22, these two antennas have nearly orthogonal current characteristics on the chassis. This orthogonality is the result of the two antennas exciting different modes on the chassis.

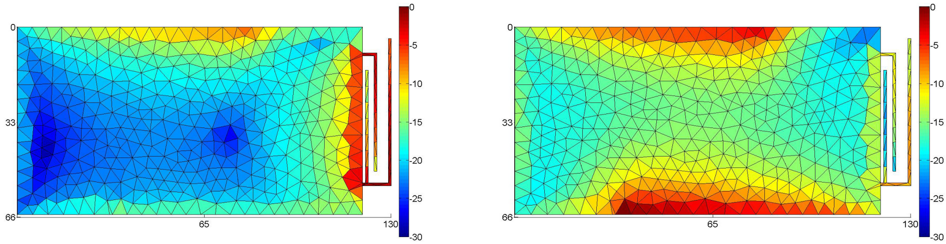

(a) (b)

Figure 22: CST current distribution with (a) monopole excited and (b) T-antenna excited

Tables 7 and 8 show the correlation and NMI between the characteristic currents and antenna currents. These tables show that the T-antenna is strongly correlated to the second mode while the monopole excites the fundamental mode more than any other modes. The relationship between the characteristic currents and antenna currents will be re-analyzed in the following chapters to find the contribution factor of each mode for each antenna port in percentage.

Table 7: T-strip prototype current correlation

Correlation	T-Antenna	Monopole
λ_1	0.15	0.84
λ_2	0.58	0.15
λ_3	0.12	0.85
λ_4	0.33	0.62

Table 8: T-strip prototype NMI

NMI	T-Antenna	Monopole
λ_1	0.09	0.4825
λ_2	0.21	0.05
λ_3	0.074	0.44
λ_4	0.18	0.33

5.2.5 Review of Current Correlation

Each table in this chapter indicates that using current distributions is not a proper solution to find the participation factor of each mode contributing to the final radiated power. This is because the characteristic currents are real currents calculated from eigenvectors. In contrast, the currents for the antenna simulations in CST were complex. Therefore, in calculating the correlations only the magnitude information is used due to the lack of phase information in the characteristic currents[3].

However, as seen in the C-Fed prototype, the actual currents on the surface of the chassis were the superposition of currents from multiple modes. If the excited modal currents are distributed differently to one another, as it was seen in the C-fed prototype, the total current forms a completely new distribution, but if the excited modes are distributed in the same directions, as it was seen in the T-strip prototype, the total current will have a similar current distribution as the excited modes. Hence, it is not always possible to find constituent modes by visual comparison of the current distribution for each excited antenna. To find the excited modes, the modal currents were analyzed.

Examination of the current distribution provides meaningful information about proper feeding methods and port location to feed a single mode or multiple modes. In addition, current analysis allows for the optimization of MIMO performance, especially correlation between the antenna elements on the ground plane of each prototype.

[3] As mentioned in Section 5.1, only the real parts (and not the magnitudes) of the currents from CST were used together with the real characteristic currents for the current correlation and the NMI calculations. This may have implication on the accuracy of the current based approach discussed in this chapter.

CHAPTER 6

6 Near-Field Simulations

Characteristic modes provide significantly more information through obtaining near-field and far-field parameters from the currents. In this chapter, the near-field information provided by CMs and CST is studied.

The information provided by near-fields can give insight into optimal placement and feeding type for coupled antenna topologies. Electric near-fields provide more information about capacitive feeds when compared to magnetic near-fields. Due to the convenient use of capacitive feeds in mobile handset antennas, including the studied prototypes, electric field analysis was considered sufficient for this research.

One of the main advantages of analyzing electric near-fields is the ease of finding excited modes. At any given frequency, the individual feeds are coupled to any resonant mode that has significant electric fields in the region of the coupling element.

6.1 TCM and CST Near-field Comparison

In this section, the methods applied in the TCM and CST programs for extracting the electric near-fields are reviewed and compared. This information was used to understand the required matching stage between the results of the two programs before any further analysis was possible.

The characteristics fields were evaluated on an isometric plane placed 15 mm above the mobile chassis. To evaluate the energy at each near-field location, the TCM program applied the dipole model. In this model, each edge element (a unit on the surface of the chassis that contains two neighboring triangles) was replaced by a Hertzian dipole. Contribution of the energy from every hypothetical dipole element is integrated over the chassis surface to calculate the total field near the terminal.

On the other hand, to get the antenna based electric fields of each prototype, a full wave simulation in CST was carried out (see Chapter 3). The CST program applied a cutting-plane to store the electric fields. To have a valid comparison, and to simplify the process of matching the data between the two programs, some initial settings were applied for the saved actual fields. The cutting-plane in CST was set at a distance of 15 mm above the mobile terminal ground plane. Steps of 1 mm on the surface of the cutting plane were considered to save the field values and ease the matching procedure.

Moreover, the cutting-plane in CST was not of the same size as the chassis, whereas the TCM program estimated the fields on a plane that was equal in size to the ground plane. Therefore, the transferred fields from CST contained excess field information, which was not available in the TCM program. The excess data were removed before the data sets were compared. To explain the reason behind the excess data, the chassis and the cutting-plane in CST are shown in Figure 23. It can be seen that the cutting-plane is limited to the bounding box, which covers a larger area than the surface of the chassis. Hence, the stored fields from CST contained data of the points that are not available in the TCM program.

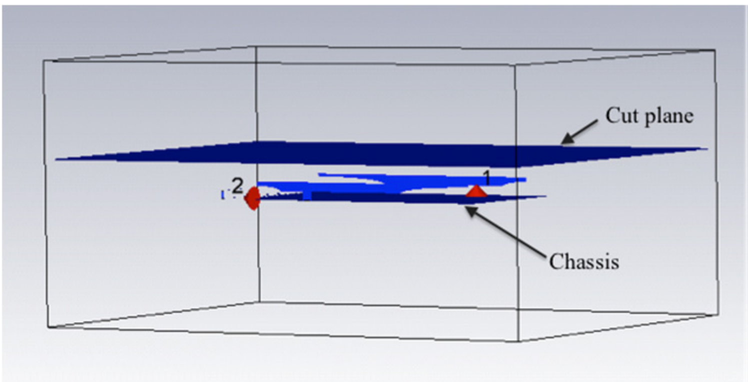

Figure 23: Cutting-plane above the chassis

To plot both TCM and CST results in Matlab, a Matlab script was developed to read the CST results first, and then it uses the geometry in the TCM results to find and remove the excess fields from the CST results. After removing the excess fields, all CST fields and characteristic fields were normalized. The reason behind normalization is that the total power in the CST and TCM programs were not equal. By analyzing the normalized field values from the CST and TCM programs, the excited modes were found.

6.2 Feed Location Study based on Electric Fields

6.2.1 Identical IFA Prototype

The CST simulated electric fields of the identical IFA prototype for port 1 are shown in Figure 24(a). Since the structure is mirror symmetric along the chassis length, the electric fields radiated by port 2 were mirror symmetric to those of port 1 and are not shown here. The figure illustrates that at the location of the feed the electric fields have the highest magnitude due to how the modes are fed. Even though only one port at a time was excited in CST, the induced fields above the other port were significant. This overlap illustrates that placing the second port opposite to the first one degrades the performance of the terminal.

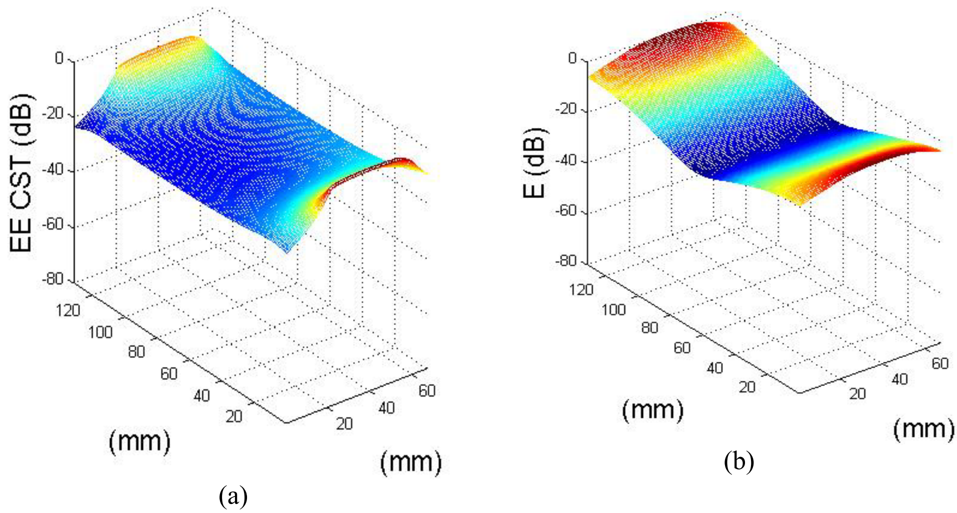

Figure 24: IFA electric fields from (a) CST simulation and (b) fundamental mode

The electric near-fields of the fundamental mode are shown in Figure 24(b). The actual fields of the chassis (Figure 24(a)) have the same behavior and are strongly correlated to this mode. According to this figure, a capacitive feed must be placed along the shorter edges of the chassis to couple into the fundamental mode. Due to the existing feed placement, both feeds easily excited the fundamental mode, inducing large coupling between the two elements. The correlation coefficient between the actual fields and the fields of the fundamental mode was 0.76. This result illustrates that the feeds were not capable of exciting the fundamental mode purely, allowing other modes to participate in the final radiated fields as well.

However, the fundamental mode is the dominant mode excited through this particular antenna placement at frequencies below 1 GHz. Other modes are not excited as much as the fundamental mode because it is more difficult to transfer energy into these modes. According to the corresponding figure of eigenvalues (Appendix 9.1), exciting λ_1 guarantees a wide resonant band.

Table 9 displays the correlation coefficient and the NMI between the CST fields and the modal fields. While the correlation coefficient shows how the modal fields were correlated to the actual ones, it does not show the exact percentage contributed by each mode. Therefore, NMI was also used as an extra metric to examine the dominant mode. This measure was not able to illustrate the exact percentage of each mode. However, after the excited modes are detected, it gives insight into which modes are excited stronger than the others. These numbers are useful together with the field analysis.

For instance, according to Table 9, λ_2 is correlated to the fields of the chassis more than λ_3. However, in order to figure out the relation of these modes with the actual fields, the modal fields should be compared to the CST fields. According to the corresponding electric field figures of λ_1 to λ_4 (Appendix 9.2) for the dual identical IFA prototype, λ_2 has high field magnitudes along the longer edges of the chassis, and low field magnitudes along the shorter edges. This information shows that this mode is unlikely to be excited by the capacitive feeds on the shorter edges, even though it is highly correlated (0.70) with the CST fields.

On the other hand, the figures predicted that the capacitive feeds were capable of exciting λ_3. The correlation factor of this mode to the CST fields is 0.59. In this example, the NMI metric in Table 9 shows that the contribution factor of the fundamental mode is significantly higher than that of λ_3 in the final CST fields.

Table 9: IFA near-field correlation and NMI

IFA	Correlation	NMI
λ_1	0.76	0.65
λ_2	0.70	0.33
λ_3	0.59	0.18
λ_4	-0.67	0

6.2.2 C-Fed Prototype

The actual electric fields of the C-Fed prototype when port 1 is excited are shown in Figure 25. This port is located at the right side of the bottom (short) edge of the chassis (see Figure 6). The field distribution of port 2 is mirror symmetric to that of port 1 due to the mirror symmetric structure of this prototype (along the chassis width).

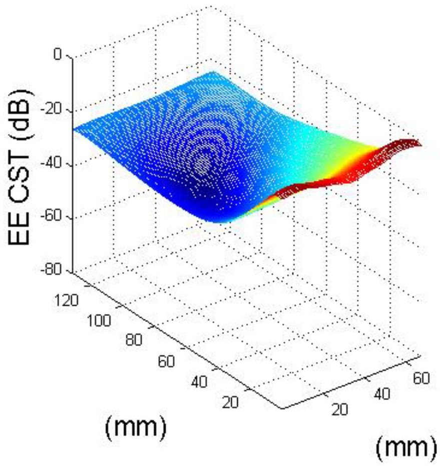

Figure 25: C-Fed electric fields from CST simulation

The actual electric fields are strongest along the short edge of the chassis where the feed of port 1 was connected. The fields marginally decrease near the middle of the bottom edge, but rise again near the location of port 2. This overlap of the electric fields from one port to the other one can be seen in Figure 25. Along the longer edges, the fields reduce first sharply and then gradually to very low values at the other shorter edge of the chassis. The near-fields drop slower on the right side of the ground plane compared to the left side, because the excited port is located on the right side. This trend can be understood by the diagonal currents that were presented in Chapter 5.

To determine the excited modes, the maximum values of the electric fields are important. Figures 26(a) and 26(b) show the electric field distributions of λ_1 and λ_2. The figures show that the fundamental mode has maximum field values at both the bottom and top shorter edges of the chassis, whereas λ_2 maintains the maximum field values along the length of the chassis; meaning that placing a feed on either of the shorter edges will excite the fundamental mode, whereas to excite λ_2 a capacitive feed should transfer the fields along the longer edges of the chassis.

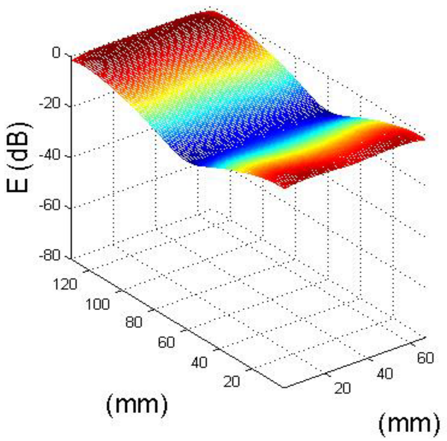

(a)

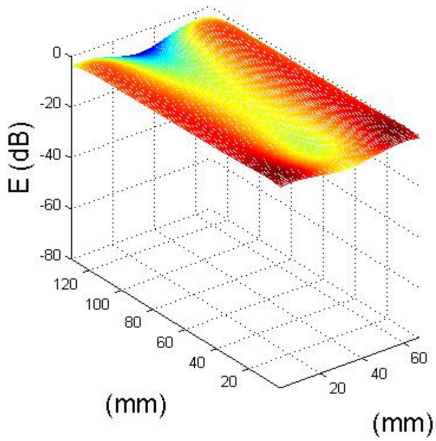

(b)

Figure 26: C-Fed modal electric fields for (a) fundamental mode λ_1 and (b) λ_2

The capacitive feeds in this prototype are located at the corners of the bottom shorter edge. Consequently, these feed placements allow for the excitation of both λ_1 and λ_2. Table 10 shows that these modes have high correlation with the CST full wave simulated fields. The fundamental mode and the second mode in Table 10 have the correlation factors of 0.72 and 0.73, respectively. These values illustrate that neither of the two modes were excited purely, and each mode only partly contributed to the final electric field distribution. According to the NMI metric, the second mode was excited more than the fundamental mode. However, these two measures of correlation and NMI do not present a clear picture of how the energy is split among these modes. Nevertheless, we can conclude that the symmetric design causes port 1 and port 2 to contribute into different modes equally.

Table 10: C-Fed near-field correlation and NMI

C-Fed	Correlation	NMI
λ_1	0.72	0.42
λ_2	0.73	0.57
λ_3	0.55	0.34
λ_4	0.37	0.52

6.2.3 PIFA-Monopole Prototype

The PIFA-Monopole prototype contains two different types of antennas. Consequently, the field distribution and participation factors of different modes are not necessarily the same for the two ports anymore. To determine the excited modes and the contribution factor of each mode, the two antennas must be evaluated separately.

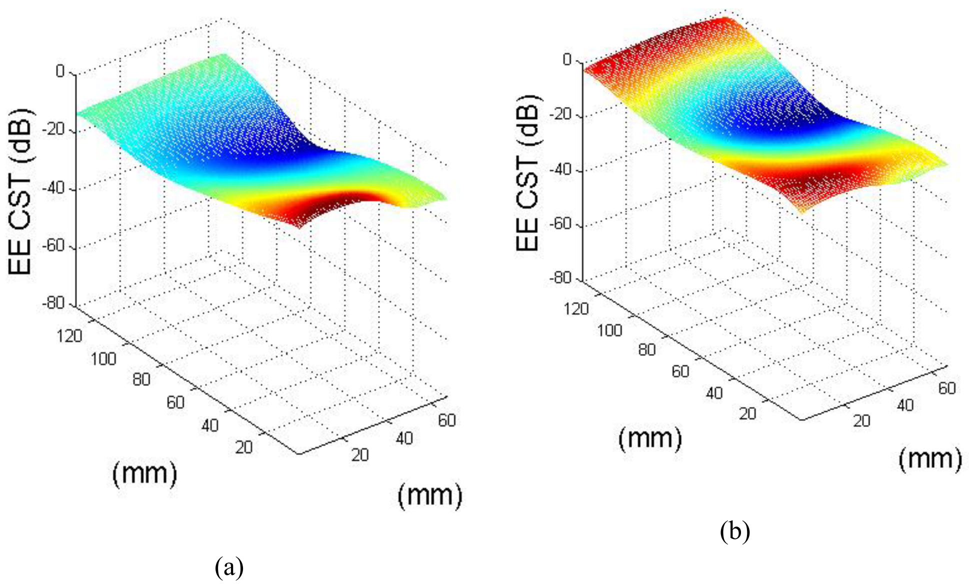

Figure 27: CST simulated electric fields for (a) PIFA and (b) monopole

Figures 27(a) and 27(b) present the CST simulated outputs with the PIFA excited and the monopole excited, respectively. According to this figure, the PIFA fields (Figure 27(a)) do not overlap with the monopole fields significantly. However, the monopole has noticeable field overlap at the location of the PIFA element. The current distribution with the PIFA excited should be localized [34] near the vicinity of the excitation structure. In the simulations, the PIFA element was located along the left side of the bottom edge, and the monopole was located along the top edge (see Figure 28).

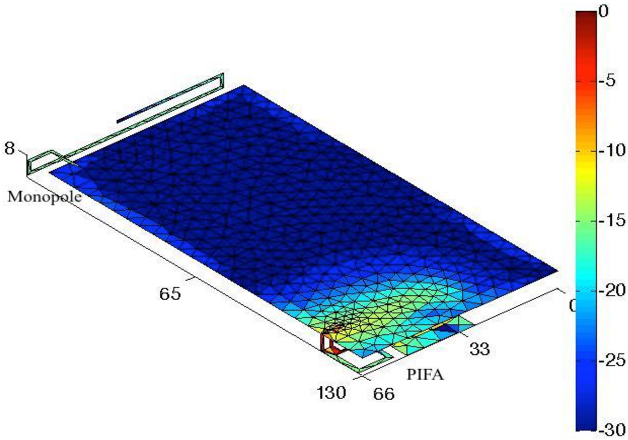

Figure 28: Location of PIFA and monopole

Modal fields of the potential resonant modes in the low band are presented in Appendix 9.2. Figure 29 shows the characteristic fields of λ_1 and λ_4 as the most likely excited modes due to their field distributions.

According to the field analysis, these two modes have strong fields along the left side of the bottom edge, which makes the PIFA capacitive feed capable of exciting these two modes. The correlation coefficients of these modes to CST simulated fields of the PIFA element were 0.63 and 0.56, respectively, which together with field analysis illustrate that the PIFA element excites both λ_1 and λ_4.

The field analysis for the monopole antenna (see Figure 27(b) and Figure 29) reveals the excitation of λ_1 and λ_4 by the monopole as well. Hence, these modes are excited by both elements connected to the ground plane. Exciting the same modes through separate ports indicates that the antenna structures are not well isolated. This is seen in Figure 27 where the field distributions of the PIFA and the monopole are clearly correlated.

It is good to recall that the IFA antennas excited the same modes equally leading to high coupling between the antenna feeds. Comparing the correlation of the ports in this prototype to the correlation of the ports in the dual identical IFA prototype shows that mounting different antenna elements on the chassis, with different radiated fields, can reduce the correlation between the ports.

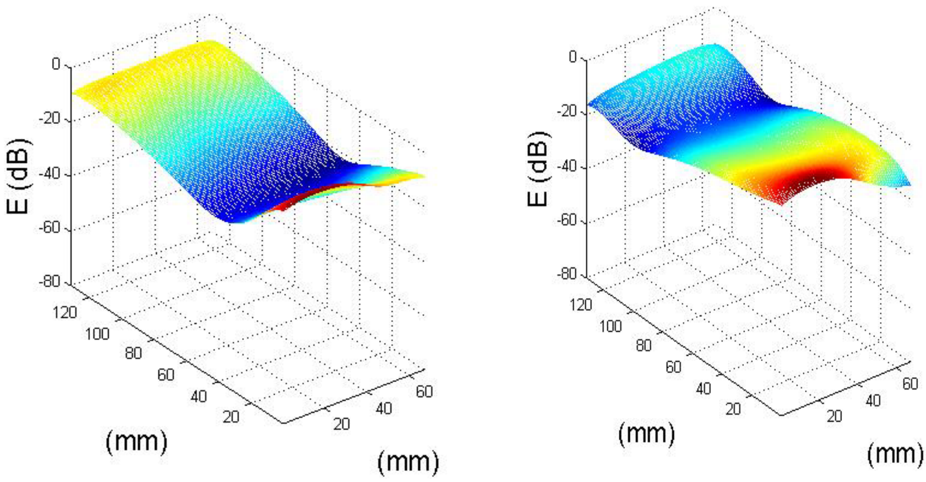

(a) (b)

Figure 29: PIFA-monopole modal electric fields for (a) fundamental mode. λ_1 and (b) λ_4

Tables 11 and 12 show the correlation coefficient and NMI between the fields of the modes closest to resonances and those of the antenna elements. According to Table 11, λ_1 and λ_4 have the highest correlation coefficient to both antennas. The monopole has higher correlation coefficient with λ_4 compared to the fundamental mode. However, the NMI measure in Table.12 shows the amount of energy coupled into mode 1 is more than mode 4. Comparing Table 11 to Table 12 implies that mode 4 is more efficiently excited in PIFA element than monopole (in terms of NMI).

Although the magnitudes of the electric fields of λ_1 and λ_4, to some extent, are similar near the bottom of the chassis, these modes have completely different magnetic fields.

The third mode is excluded from the results in Table 11 due to the mode never becoming a resonant mode (red line in Figure 30).

Table 11: PIFA near-field correlation and NMI

PIFA	Correlation	NMI
λ_1	0.63	0.56
λ_2	0.3	0.30
λ_4	0.56	0.48
λ_5	0.34	0.66

Table 12: Monopole near-field correlation and NMI

Monopole	Correlation	NMI
λ_1	0.6	0.55
λ_2	0.3	0.23
λ_4	0.64	0.44
λ_5	0.12	0.48

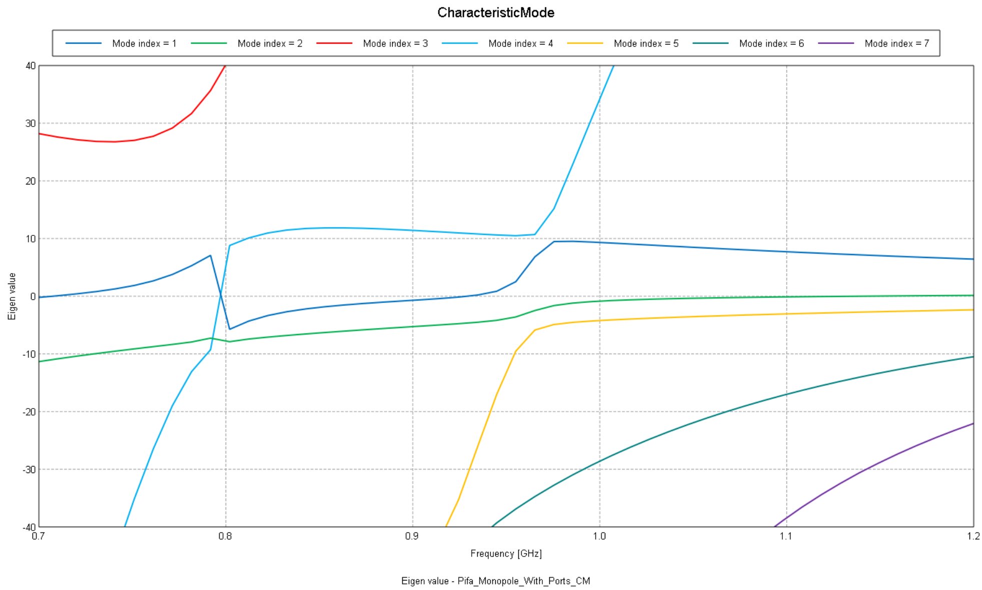

Figure 30: Eigenvalues of PIFA-monopole prototype

T-Strip Antenna Prototype

Chapter 4 explained the design of the T-strip antenna prototype based on the characteristic modes. This antenna presents unique results when discussed from a near-field point of view because it is designed to excite different modes by different ports. This design is an effort to purely excite different characteristic modes [9]. Figures 31(a) and 31(b) show the electric near-fields of the monopole and T-antenna, respectively. The highest fields of the monopole and the T-antenna are approximately 90 degrees apart (about the chassis center). The T-antenna distributes the electric fields along the length of the chassis, whereas the monopole fields are distributed along the width.

The fundamental mode and the second mode of the chassis are shown in Figure 31. λ_1 has elevated values along the top and bottom short edges. Since the monopole is located at the top edge and was fed capacitively, it excites the fundamental mode of the chassis as the main resonant mode. The correlation between this mode and the monopole element is calculated to be 0.64 (see Table 13), which indicates that the feed is coupled to modes other than the fundamental mode too. The NMI metric shows that the monopole's electric fields contained information from the second mode as well. The modal fields of λ_1 and λ_2 are presented in Figure 32. Since the monopole feeding strip was not located at the middle of the shorter edge, where λ_2 is at the minimum value, the feed is capable of exciting λ_2 as well.

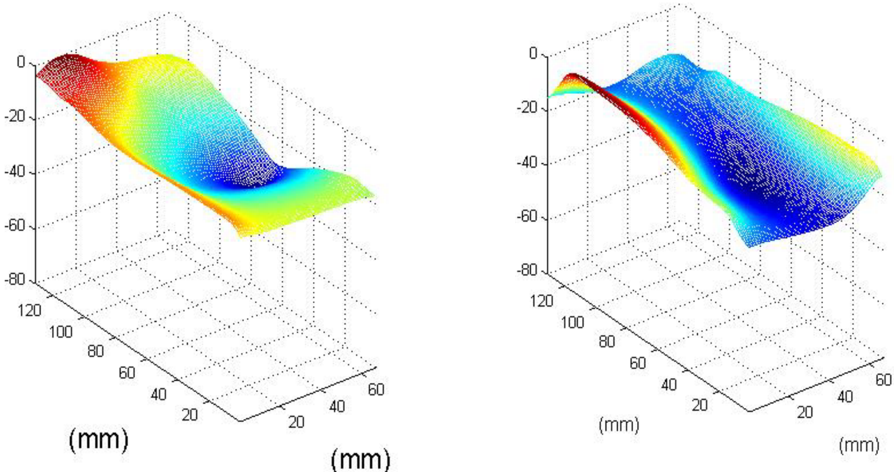

(a) (b)

Figure 31: CST electric fields for (a) monopole excited and (b) T-antenna excited

The second port is a current-fed T-antenna. Due to the capacitive excitation, high fields can be seen on a longer edge in Figure 31(b). This distribution is correlated to λ_2 with the correlation factor of 0.75. Although this factor implies that λ_2 is the dominant mode, it also shows that it is not fed purely. Only a correlation factor of approximately 1 means the feed has excited the given mode exclusively. Otherwise, several other modes also contribute to the total fields produced by port 2 on the chassis. Table 14 shows that the T-antenna port excites λ_4 as well. Appendix 9.2 presents the fields of this mode, which also has high fields on the longer edges.

A comparison between Tables 13 and 14 indicates that these ports excite different modes as the main sources of energy but they also show that the ports are not perfectly coupled into separate modes. This is because the feeds are not located exactly in the middle of the respective edges; therefore each port also coupled into other modes. It was described in [9] that exciting multiple modes is used in the T-antenna to enhance the resonant bandwidth in the low band.

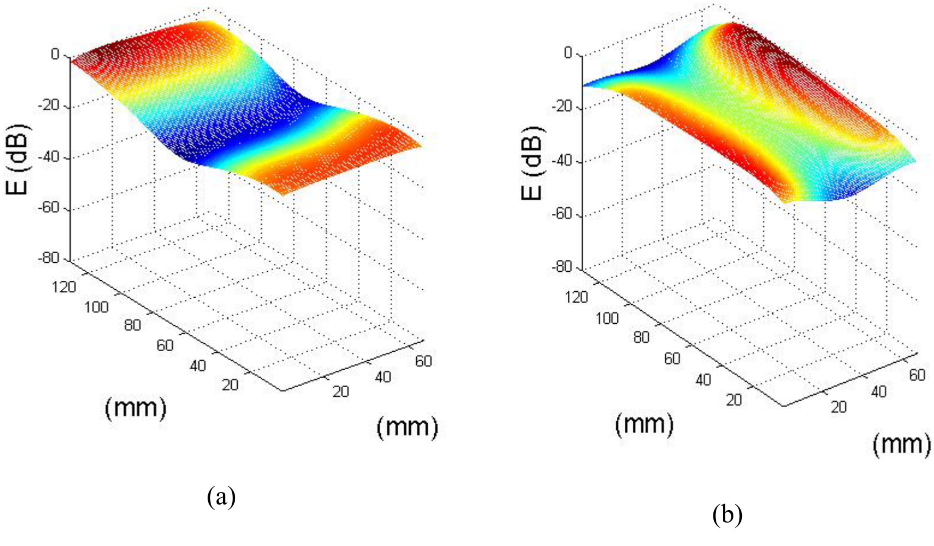

Figure 32: Modal fields for (a) fundamental mode λ_1 and (b) λ_2

The impact of exciting the second mode by both ports is not destructive to the total electric fields. The two ports have different dominant modes and the coupled modes may be fed at different polarizations, this was seen in the

C-Fed as well. Therefore, the resulting characteristics are nearly orthogonal with a far-field envelope correlation coefficient of less than 0.05.

Table 13: Monopole near-field correlation and NMI

Monopole	Correlation	Mutual information
λ_1	0.64	0.69
λ_2	0.34	0.63
λ_3	0.3	0.51
λ_4	0.3	0.3

Table 14: T-antenna near-field correlation and NMI

T-antenna	Correlation	Mutual information
λ_1	0.1	0.11
λ_2	0.75	0.64
λ_3	0.33	0.45
λ_4	0.68	0.61

6.2.4 Further Explanations

The analysis of the electric fields is important in finding the excited modes and to find out a proper location on the chassis to excite a given mode. It is also useful to study whether a group of modes could be fed simultaneously by a single port or not and what is the proper location on the chassis to place such a feed.

However, the near-field analysis does not provide the desired contribution factor of each mode because the TCM program used only the magnitude of the fields whereas the CST fields of the antennas are inherently in complex form.

CHAPTER 7

7 Far-Field Simulations

In this chapter, the magnitude and phase information that lies in the far-fields were used to estimate the contribution of each mode in the radiated pattern. The ECC between the excited antenna radiation pattern and the characteristic far-fields presents the contribution factor of each characteristic mode in the radiated pattern.

This chapter contains two main sections. In the first section, prototypes without dielectrics were simulated in CST and the results were correlated to the modal far-fields without dielectrics. In the second part, the dielectrics were added back to the CST models. The ECC was calculated between the radiated far-fields with dielectrics and the modal far-fields without dielectrics.

7.1 Initial Settings in FEKO and CST

Characteristic far-fields were simulated in EMSS FEKO. The results were transferred to Matlab where they were correlated to the full-wave simulated far-fields in CST. However, an initial setup was applied in both programs before saving the results in order to simplify the analysis and avoid unnecessary matching between the coordinate systems of the two programs.

The chassis were oriented in the same directions manually in FEKO and CST. Before simulating the models, the local coordinate centers were aligned in both programs. Consequently, as was explained in Chapter 4, no additional matching was required between the simulated results in CST and FEKO.

7.2 Far-Fields Analysis

7.2.1 Far-Fields Analysis without Dielectrics

The first studied prototype was the dual IFA prototype as described in the previous chapters. Figures 33(a) and 33(b) show the radiation patterns of ports 1 and 2, respectively. These patterns are nearly identical, with only a slight tilt in angle differentiating the two patterns. The pattern similarity degrades the MIMO performance of the prototype. The far-field pattern of the fundamental mode of this prototype is presented in Figure 33(c). Visual comparison of the characteristic far-field pattern to the far-field antenna patterns shows that the radiated power of both ports has significant contribution from the fundamental mode.

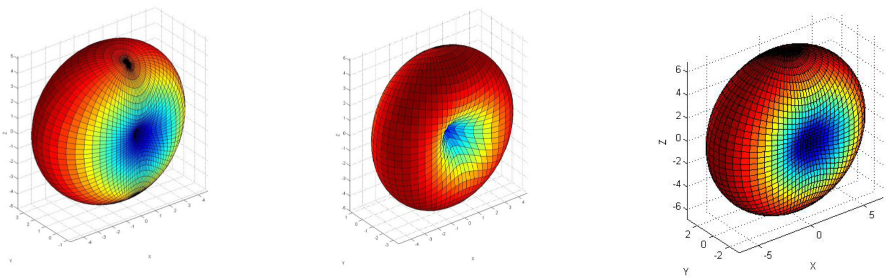

(a) (b) (c)

Figure 33: IFA prototype far-field patterns for (a) port 1, (b) port 2, (c) fundamental mode

In order to investigate the contribution of different modes accurately, the EEC value between each antenna pattern and the characteristic far-field pattern was evaluated. The results are presented in Table 15. A quick comparison between the columns of port 1 with port 2 indicates that due to the symmetry of the structure and the mirrored locations of the feeds, the ECC of port 1 to any given modal pattern is nearly equal to the ECC of port 2 to that mode, which means the energy transferred to a given mode by port 1 is nearly identical to the energy transferred by port 2.

The fundamental mode, as was expected from Chapters 5 and 6, is the dominant mode in the final radiated patterns of both ports. The contribution factor of the fundamental mode is approximately 69%. According to the table, λ_3 is the second most excited mode and it provides almost 20% of the total radiated power. The considerable contribution of this mode was also correctly predicted in the previous chapters. These factors illustrate that the

IFA elements transfer almost 89% of the total power to λ_1 and λ_3. Hence, these two modes are sufficient to describe the radiation behavior of the IFA elements.

In Table 15 the contribution factor of λ_2 is effectively zero. The reason behind this is that the excited patterns are almost orthogonal to the pattern of this mode, which can be seen in Appendix 9.2.

Table 15: IFA prototype mode participation in far-field

IFA	Port 1	Port 2
λ_1	0.6931	0.6953
λ_2	6.1973e-04	5.5972e-04
λ_3	0.2086	0.2075
λ_4	0.0698	0.0688
λ_5	0.0182	0.0181
λ_6	0.0085	0.0085

The second studied prototype was the C-Fed prototype with two identical antennas. The physical shapes of the excited radiation patterns are the same in general, since the chassis is fully symmetric. Figure 34 shows the CST simulated far-field patterns of port 1 and port 2. As the figure indicates, the two patterns are more tilted away from one another as compared to those of the dual identical IFA prototype. Thus, the patterns are better isolated in the C-Fed model.

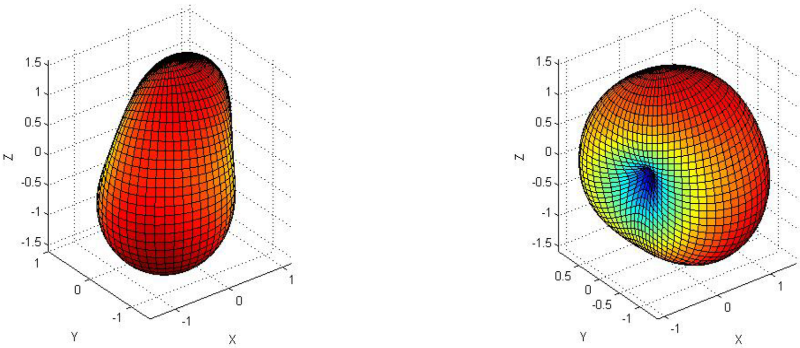

(a) (b)

Figure 34: C-Fed prototype far-field pattern for (a) port 1 and (b) port 2

Comparing the radiated patterns to the modal fields (Appendix 9.2) shows that each radiated pattern does not correspond to only one mode. The detailed study of the excited modes according to the location of the feed, like the field analysis in Chapter 6, was not possible in the far-field because the far-field patterns were solved at a considerable distance from the chassis.

However, the ECC illustrates how combining separate modes has formed the radiated far-field pattern of each port. Table 16 shows the percentage of the transferred power from each mode in the final excited structure (with port 1 or 2 excited). Once again, due to the symmetry of the structure, both ports excite the same modes. The dominant radiated fields are concentrated to two modes closest to resonance in the band of interest. This was predicted in Chapter 6 as these two modes have high electric fields at the corners. Hence, if a capacitive feed is placed there, it should excite both modes. The patterns of these modes are presented in Figure 35(a) and 35(b).

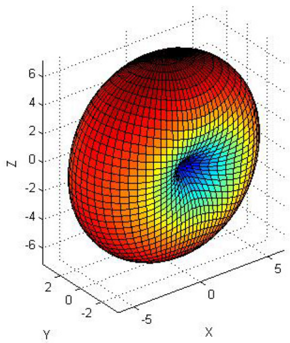

(a)

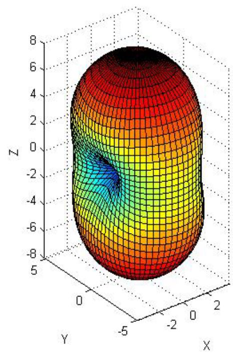

(b)

Figure 35: C-Fed prototype far-field patterns for (a) mode 1 and (b) mode 2

According to Table 16, λ_2 transfers more power to the excited fields as compared to the fundamental mode. These two modes together supply more than 70% of the total radiated power, indicating that they may be another mode that effectively contributes to the radiation. Indeed, the table shows that in this design, λ_5 was also significantly excited.

Table 16: C-Fed prototype mode participation in far-field

C-Fed	Port 1	Port 2

λ_1	0.2067	0.2312
λ_2	0.4808	0.4662
λ_3	0.0016	4.9869e-04
λ_4	0.0545	0.0574
λ_5	0.1673	0.1810
λ_6	0.0261	0.0022

In Chapters 5 and 6, the excited modes of each port in the PIFA-Monopole prototype were predicted. It was seen that both antennas were strongly exciting the fundamental mode. However, since this prototype contains two different antenna types, the field contribution of the fundamental mode to each antenna is expected to be different.

The radiation patterns of each antenna as well as the fields of the fundamental mode are shown in Figure 36. Because both antennas are highly coupled to the fundamental mode, the physical appreance of the two radiated patterns are not significantly different.

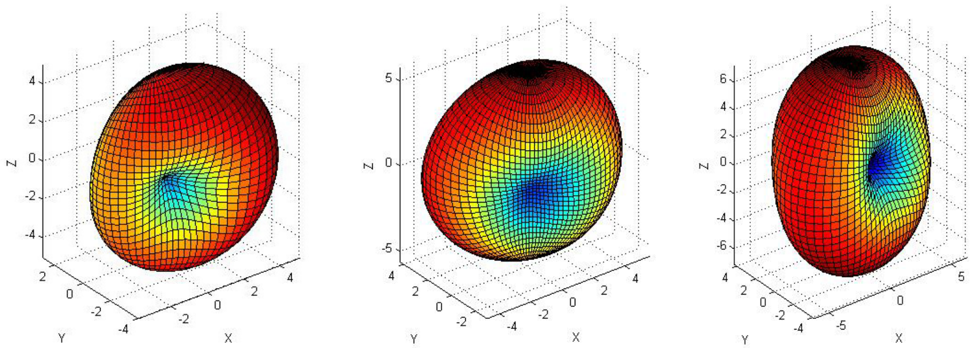

(a) (b) (c)

Figure 36: PIFA-monopole prototype far-field patterns for (a) monopole, (b) PIFA, and (c) fundamental mode

The calculated ECC values between the excited far-field patterns and the modal patterns in the far-field prove the prediction about the dominant mode and the contribution factors. The total modal contributions of the PIFA-monopole prototype were calculated, and presented in Table 17. According to this table, the fundamental mode supplies 55% of the total power in the PIFA element and 68% percent of the total power in the monopole element, respectively.

According to Table 17, both antenna elements excite λ_4 as well. This was also predicted in current and near-field analysis. The contribution factor of λ_4 is 28% for the PIFA and only 11% for the monopole. The modal far-field patterns of this prototype (for λ_1 to λ_6) are presented in Appendix 9.2.

Table17: PIFA-monopole prototype mode participation in far-field

PIFA-monopole	PIFA	Monopole
λ_1	0.5572	0.6835
λ_2	0.1128	0.0165
λ_3	0.0327	0.0754
λ_4	0.2883	0.1146
λ_5	0.0024	0.0134
λ_6	0.0045	0.0274

The final analyzed prototype was the T-strip prototype. The excited patterns of the T-antenna and the monopole antenna are shown in Figures 37(a) and 37(b), respectively. Since the antenna patterns of the prototype in this figure are oriented nearly perpendicularly, they should be highly isolated. The modal fields of the first and second modes are presented in Figure 38. A comparison between Figures 37 and 38 suggests that the monopole antenna is mainly exciting λ_1, whereas the T-antenna is highly correlated with λ_2.

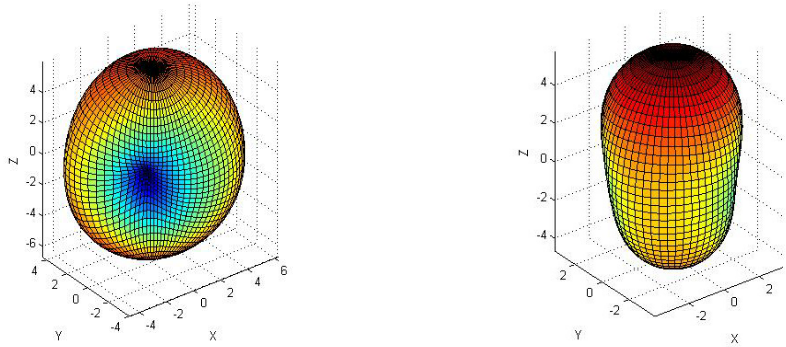

(a) (b)

Figure 37: T-strip prototype far-field pattern for (a) monopole and (b) T-antenna

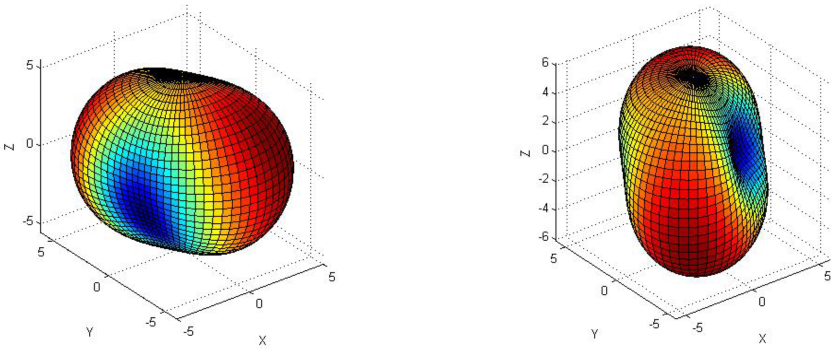

(a) (b)

Figure 38: T-strip prototype far-field patterns for (a) fundamental mode and (b) mode 2

Table 18: T-strip prototype mode participation in far-field

T-shape	T-antenna	Monopole
λ_1	0.2271	0.5637
λ_2	0.5490	0.2813
λ_3	0.0223	0.0958
λ_4	0.1837	0.0508
λ_5	0.0033	7.5906e-05
λ_6	0.0097	0.0038

The excited modes were evaluated by means of far-field ECC between excited fields and modal fields and the results are shown in Table 18. Table 18 shows that this prototype does not fully excite separate modes of operation. However, the similar modes that were excited by both ports were excited out of phase from one another and thus the ECC between the excited fields is extremely low.

7.2.2 Far-Fields Analysis with Dielectrics

As mentioned in Section 4.2, all dielectrics were removed in this study to simplify TCM calculations. In this section, dielectrics were added back to the prototypes in CST. The models were then re-analyzed as before using far-field correlation. The reason to bring back the dielectrics is to investigate the impact of removing dielectrics on the TCM in antenna design. The modal fields used in this section are the same modal patterns used in Section 7.2.1, in which the dielectrics were neglected. Tables 19 through to 22 show the contribution factors of the antenna ports in the different prototypes to the first six low order characteristic modes.

Table 19: IFA prototype (with dielectrics) mode participation in far-field

IFA	Port 1	Port 2
λ_1	0.6747	0.6772
λ_2	1.9225e-04	1.4855e-04
λ_3	0.1804	0.1813
λ_4	0.0980	0.0950
λ_5	0.0328	0.0326
λ_6	0.0130	0.0130

Table 20: C-Fed prototype (with dielectrics) mode participation in far-field

C_Fed	Port 1	Port 2
λ_1	0.8188	0.8254
λ_2	0.1595	0.1554
λ_3	9.5648e-04	1.5421e-04
λ_4	0.0058	0.0090
λ_5	0.0109	0.0106
λ_6	3.8308e-05	4.5746e-05

Table 21: PIFA-monopole prototype (with dielectrics) mode participation in far-field

PIFA-monopole	PIFA	Monopole
λ_1	0.8448	0.7393
λ_2	0.0471	0.0202
λ_3	0.0083	0.1219
λ_4	0.0059	0.0127
λ_5	0.0160	0.0725
λ_6	0.0723	0.0219

Table 22: T-Strip prototype (with dielectrics) mode participation in far-field

T-shape	T-antenna	Dipole
λ_1	0.6021	0.4908
λ_2	0.3736	0.4602
λ_3	0.0191	0.0150
λ_4	0.0022	0.0105
λ_5	4.5899e-04	0.0169
λ_6	0.0020	3.6207e-05

An overall comparison of the information provided in Tables 19 to 22 against those in Tables 15 to 18 illustrates the effects of dielectrics on the characteristic modes of each structure. This comparison shows how the use of dielectrics (with corresponding dielectric constants) affects the CM contribution. Using more dielectrics can have a large effect on the radiation properties and the excited modes. To clarify this, we take the IFA prototype and the C-Fed prototype and examine the impact of dielectrics in each structure.

The IFA prototype, with dielectrics, is shown in Figure 39. There is only a small amount of dielectric material in this structure (i.e. FR4 layer on the ground plane and a thin shell of antenna carrier at both shorter edges). Thus, the removal of dielectrics did not strongly affect the excited modes. Table 19 shows the mode contribution after adding the dielectrics to the prototype. According to this table, the dielectrics change the excitation factor of different modes, including the dominant mode, and they may also change the properties of the characteristic modes (if calculated with the dielectrics). However, these changes are not significant in this particular prototype.

On the other hand, the C-Fed prototype relies on the dielectric material to operate properly. Therefore, the dielectrics have a significant impact on the characteristic modes in this model. In Section 7.2.1, it was shown that λ_1 and λ_2 were both participating strongly in the radiated fields of the excited antennas. Table 20 reveals that the dielectrics increased the participation factor of the fundamental mode to more than 80%, which left only a small portion of the radiated field utilizing the second mode. The significant effect of dielectrics on the dominant mode could explain why the structure maintains a higher bandwidth potential with dielectrics than without. The C-Fed prototype with and without dielectrics is shown in Figures 40(a) and 40(b).

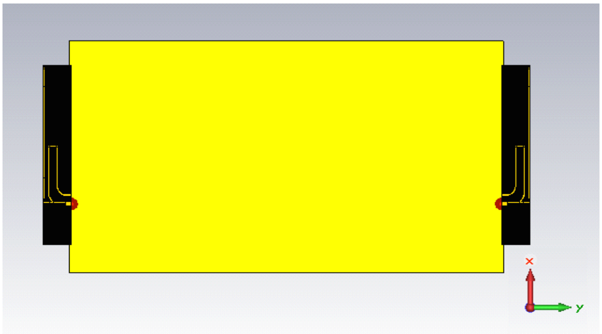

Figure 39: Dielectrics below the ground plane of IFA prototype

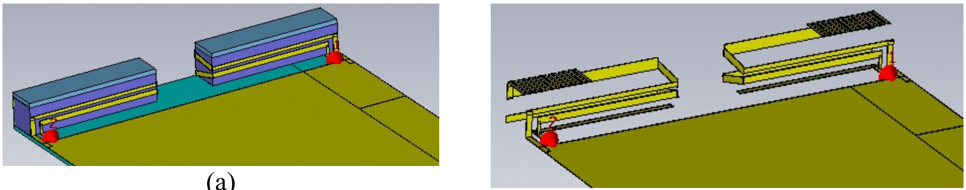

(a) (b)

Figure 40: C-Fed prototype (a) with dielectrics and (b) without dielectrics

In Tables 19 and 20, the contribution of a given mode to either of the antennas is approximately equal due to the symmetry of the prototypes. Tables 21 and 22 show different correlations for the two ports, since in these prototypes different antennas were connected to the ground plane.

Table 22 shows the correlation results for the T-strip prototype with the addition of dielectrics. Adding the dielectrics to this prototype has weakened the excitation of separate modes. Consequently, despite that the dielectrics increase the computational complexity to solve TCM problems, considering them in TCM calculations is important to achieve a more complete understanding of the characteristic modes.

CHAPTER 8

8 Summary of the Results

This research focused on the excitation of characteristic modes in multi-antenna handsets. The characteristic currents, near-fields, and far-fields of different mobile antennas were analyzed. The appropriate locations of the ports on the chassis to excite selective modes were determined through current distributions and near-fields analysis.

The current distributions of the excited modes are useful tools to study the induced currents on a chassis due to port excitation. Therefore, through current analysis, the isolation of the antenna elements connected to the ground plane was investigated for each prototype. For instance, it was seen that the antennas on the T-strip prototype maintained perpendicular current distributions along the shorter and longer edges of the chassis, leading to decoupled elements. For the C-Fed prototype, exciting the feeds provided different diagonal current distributions, which offered higher isolation compared to the elements in the IFA prototype.

Moreover, studying characteristic current distributions provided crucial information on the excitability of arbitrary modes using a certain feeding method. The optimum location for single- and multi-mode excitation can be found through examining characteristic currents. The reason behind the current distribution induced on each prototype was understood according to the excited modes, like the diagonal currents in C-Fed, which was obtained as a result of the partial excitation of the two modes closest to resonance.

Broadly speaking, the fundamental mode in each prototype was excited effectively by all elements, with the exception of the T-antenna. This common feature of all the elements exciting this mode is a reflection of the ease of transferring energy into it. Even the T-antenna, which was purposely designed to avoid exciting this mode, still excites the fundamental mode to a significant extent (especially when dielectrics are added). However, the ECC between the antenna elements was still low. The attempt to feed separate modes in the T-antenna was made by proper feed placement.

Alternatively, all positions of possible electric and magnetic feed points can be found through near-field analysis. The proper positions to excite selective modes can be conveniently investigated by studying the modal fields, which is important in antenna design since each feed normally excited multiple modes, either to increase the resonant bandwidth, as was done in [9], or to increase the isolation between antennas. Take for example, in the PIFA-monopole prototype, the excitation of λ_4 was correctly predicted through examining the electric field distributions. In addition, in the IFA prototype, the high isolation between the elements and λ_3 was discovered.

The fundamental mode in all the studied prototypes showed the same electric field behavior. According to the profile appearance of the modal fields, in order to excite the fundamental mode in all the studied prototypes, a capacitive feed should be placed on a shorter edge of the chassis, whereas a capacitive feed should be placed on a longer edge to excite λ_2.

Furthermore, the far-fields were also investigated to find the excited modes. Excited modes based on the far-field analysis were the same modes that were predicted by analyzing the currents and near-fields. This analysis provided the contribution of each mode in the excited patterns, which is useful to understand the performance of the multiple-antenna handsets. However, far-field analysis could not be used to find proper feed placement or excitation type, due to the far-field patterns being evaluated far away from the prototypes. To find the proper feed position and feeding method, the information on the near-fields and current distributions are still required.

Finally, this project analyzed the electric near-fields, and not the magnetic near-fields, due to the majority of the prototypes relying on capacitive coupling elements for excitation. As one possible future work, each terminal prototype can be analyzed using the magnetic near-fields as well as the capacitive near-fields. A larger range of terminal prototypes, including those using inductive coupling elements (ICEs), may also be considered for future study.

9 Appendix

9.1 Resonant Modes of Different Prototypes

I. Ground-plane of dimensions 130 mm × 65 mm:

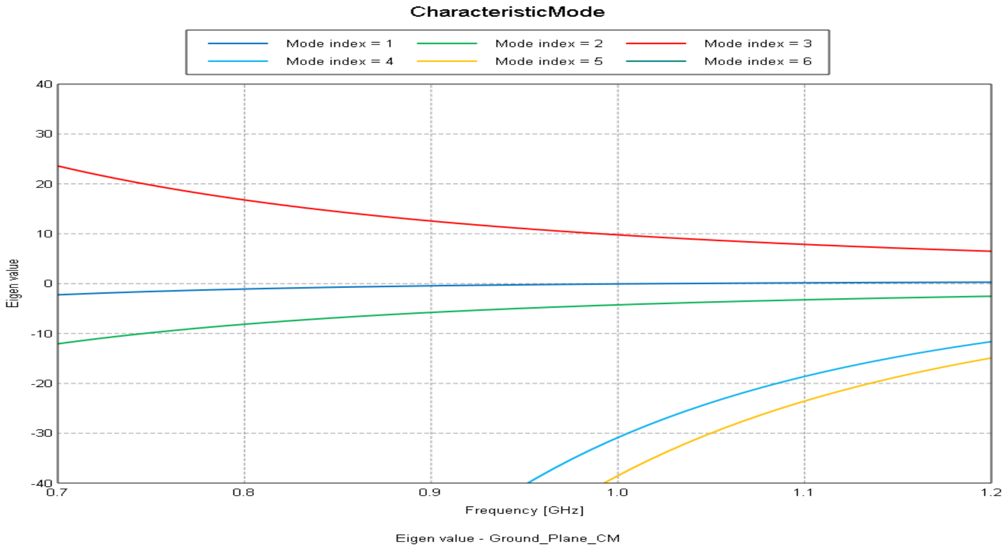

Figure 9.1: Characteristic eigenvalues of a 130 mm × 65 mm ground-plane

II. IFA Prototype:

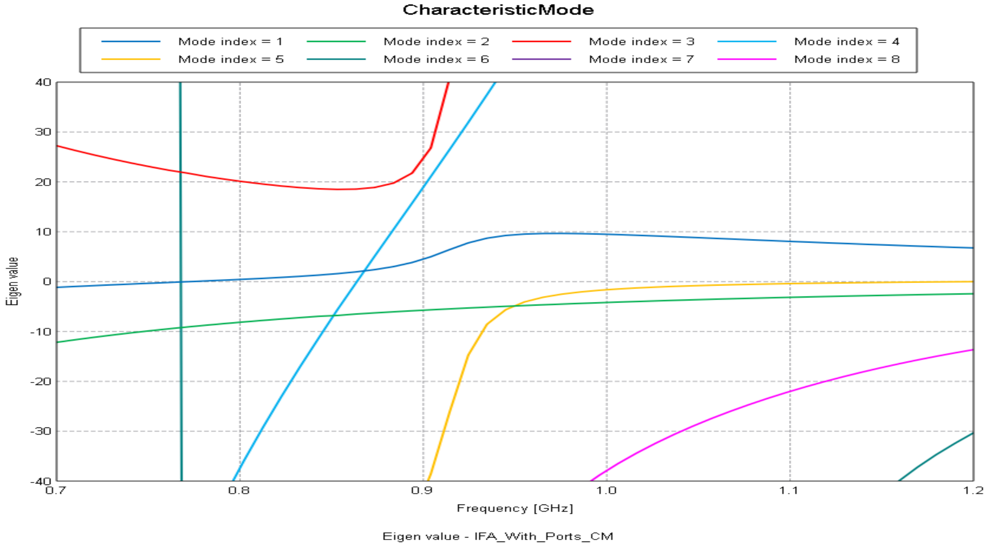

Figure 9.2 Characteristic eigenvalues of dual identical IFA prototype

III. C-Fed Prototype:

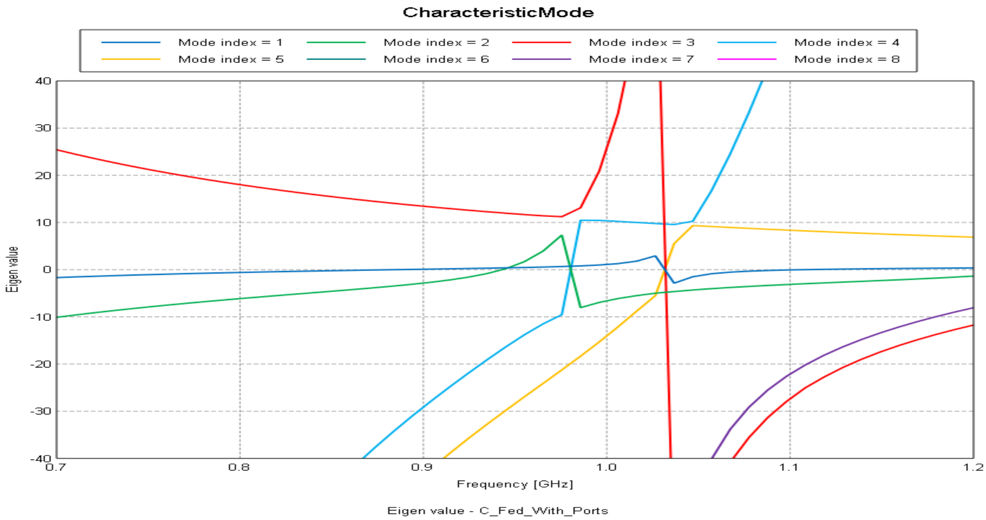

Figure 9.3 Characteristic eigenvalues of C-Fed prototype

IV. PIFA-monopole Prototype:

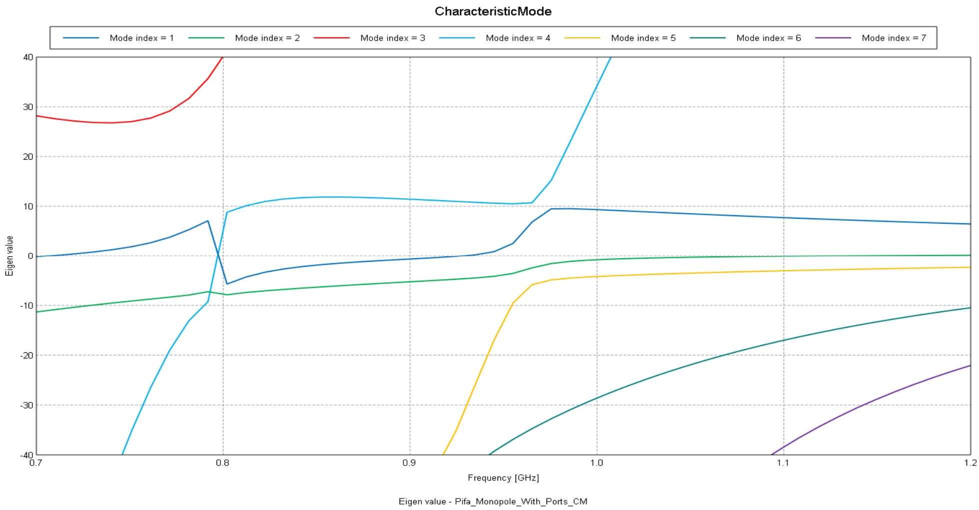

Figure 9.4: Characteristic eigenvalues of PIFA-monopole prototype

V. T-Strip Prototype:

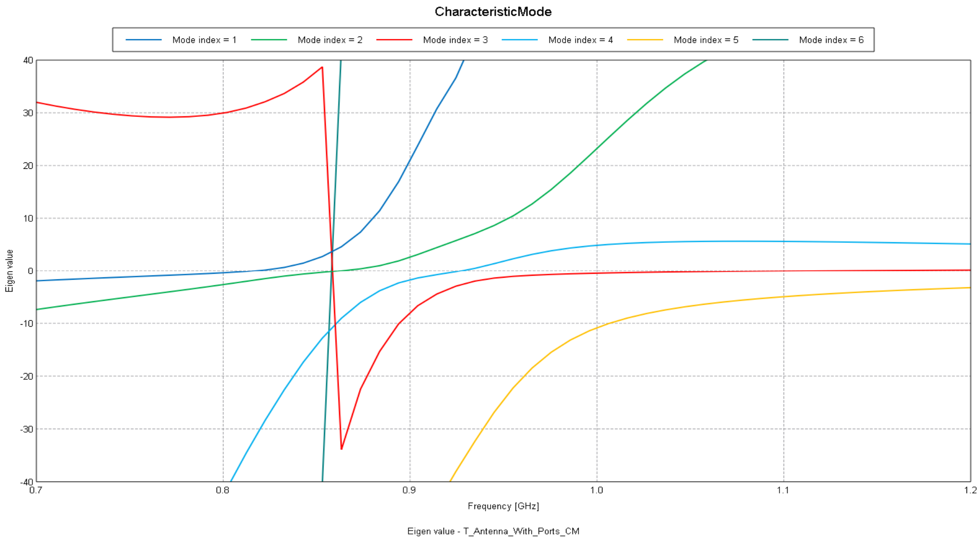

Figure 9.5: Characteristic eigenvalues of T-strip prototype

9.2 Characteristic Currents and Fields

I. IFA Prototype:

1. Current Distributions:

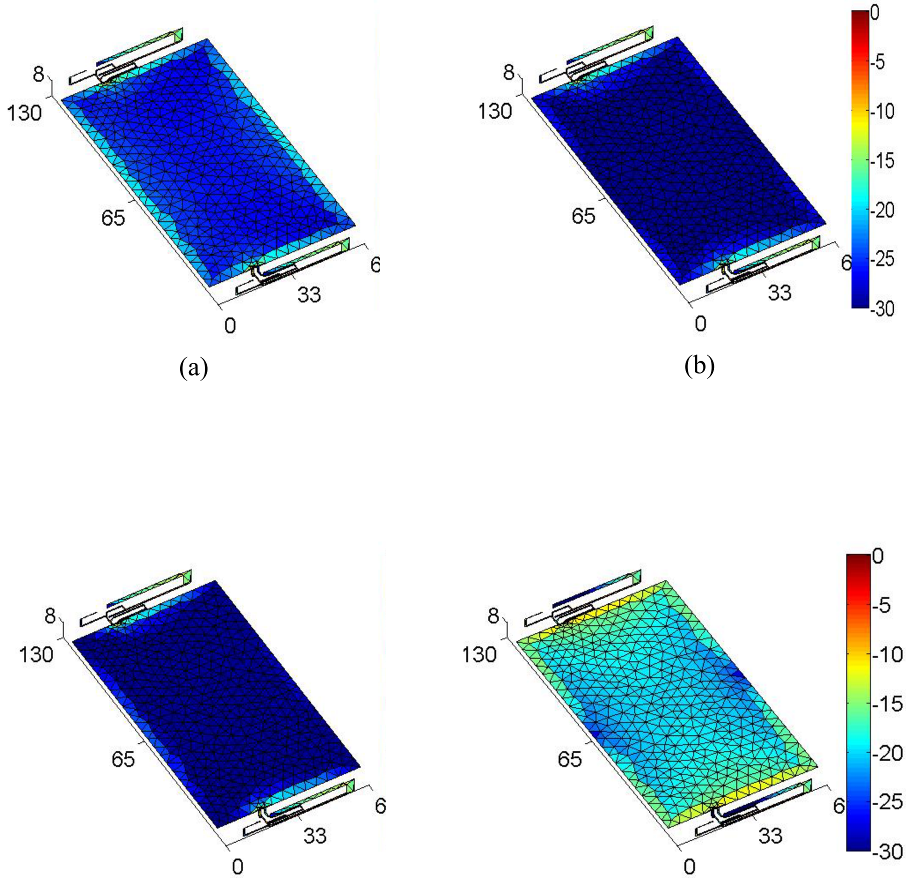

(a) (b)

(c) (d)

Figure 9.6: IFA prototype modal current distributions for (a) mode 1, (b) mode 2, (c) mode 3, and (d) mode 4

2. Near-Fields:

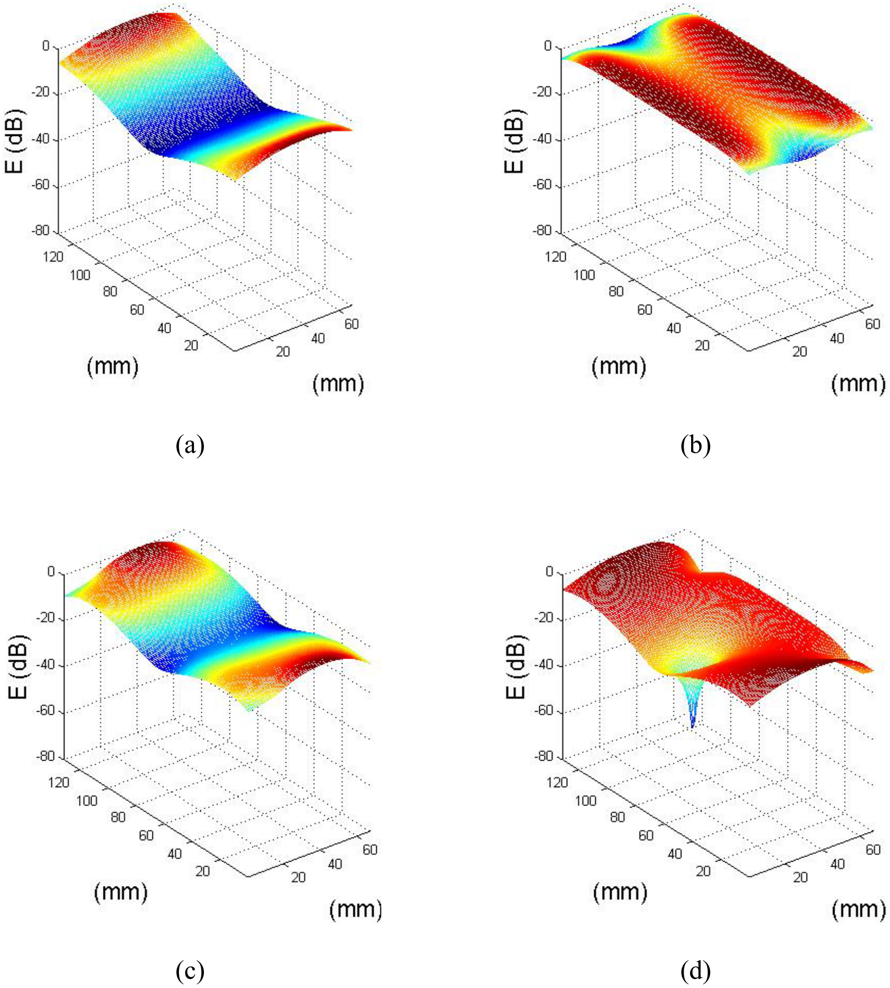

Figure 9.7: IFA prototype modal electric near-fields for (a) mode 1, (b) mode 2, (c) mode 3, and (d) mode 4

3. Far-Fields:

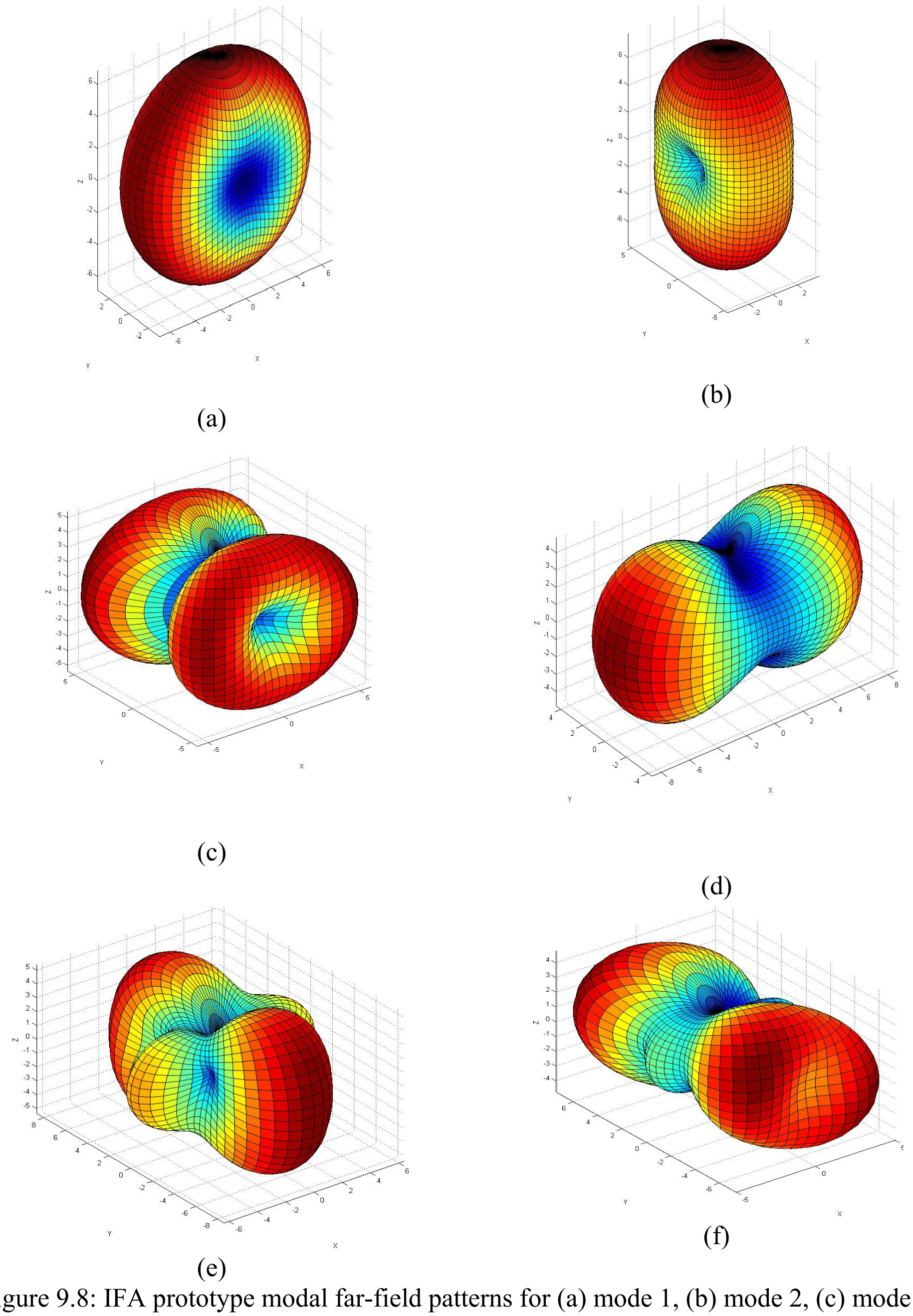

Figure 9.8: IFA prototype modal far-field patterns for (a) mode 1, (b) mode 2, (c) mode 3, (d) mode 4, (e) mode 5, and (f) mode 6

II. C-fed Prototype:

1. Current Distributions:

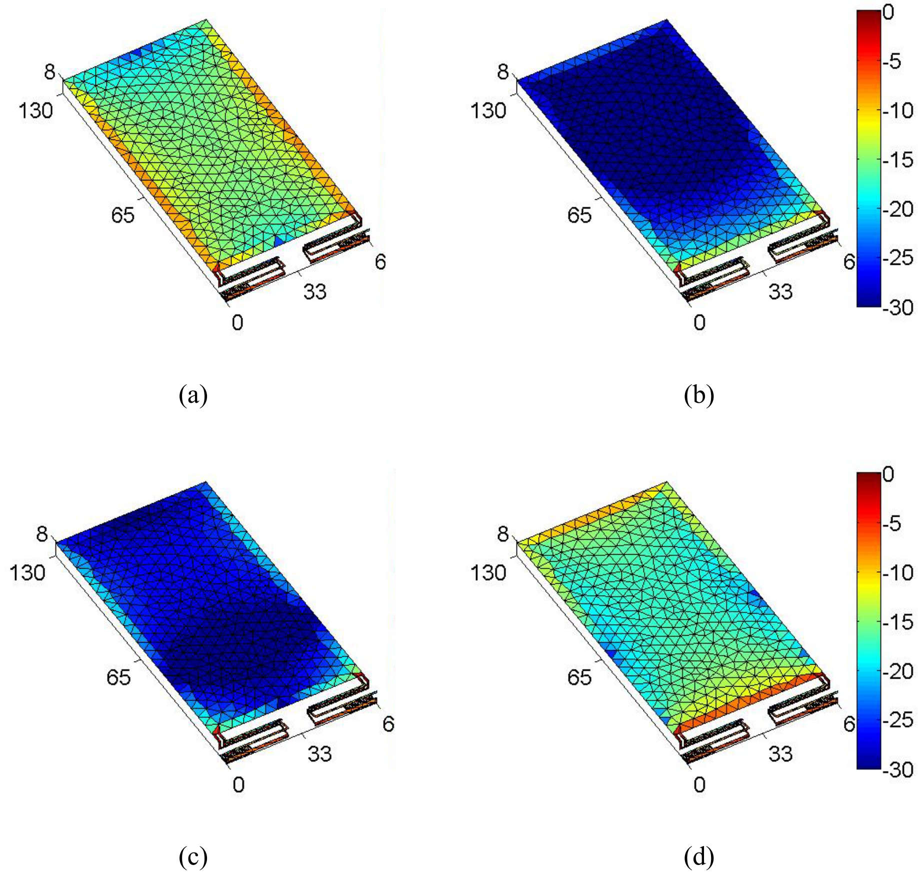

Figure 9.9: C-Fed prototype modal current distributions for (a) mode 1, (b) mode 2, (c) mode 3, and (d) mode 4

2. Near-Fields:

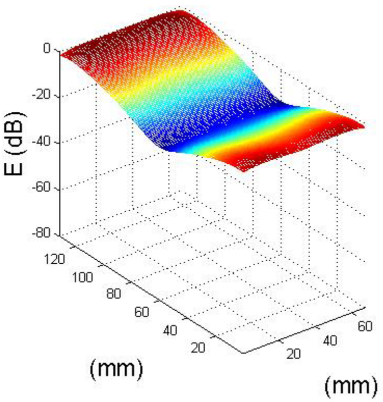

(a)

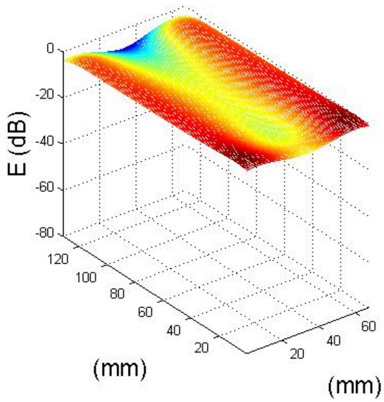

(b)

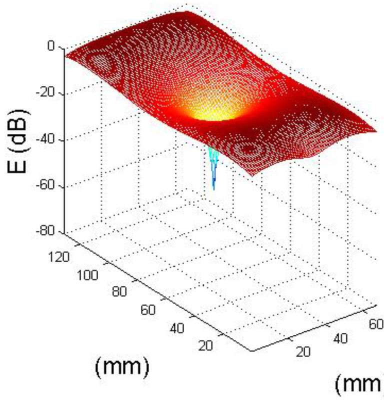

(c)

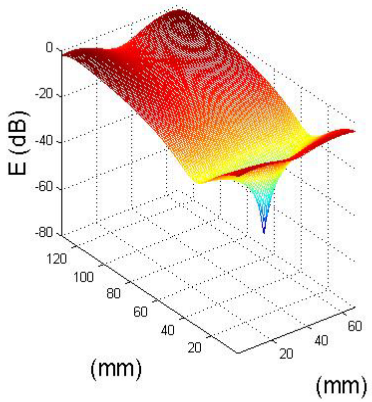

(d)

Figure 9.10: C-Fed prototype modal electric near-fields for (a) mode 1, (b) mode 2, (c) mode 3, and (d) mode 4

3. Far-Fields:

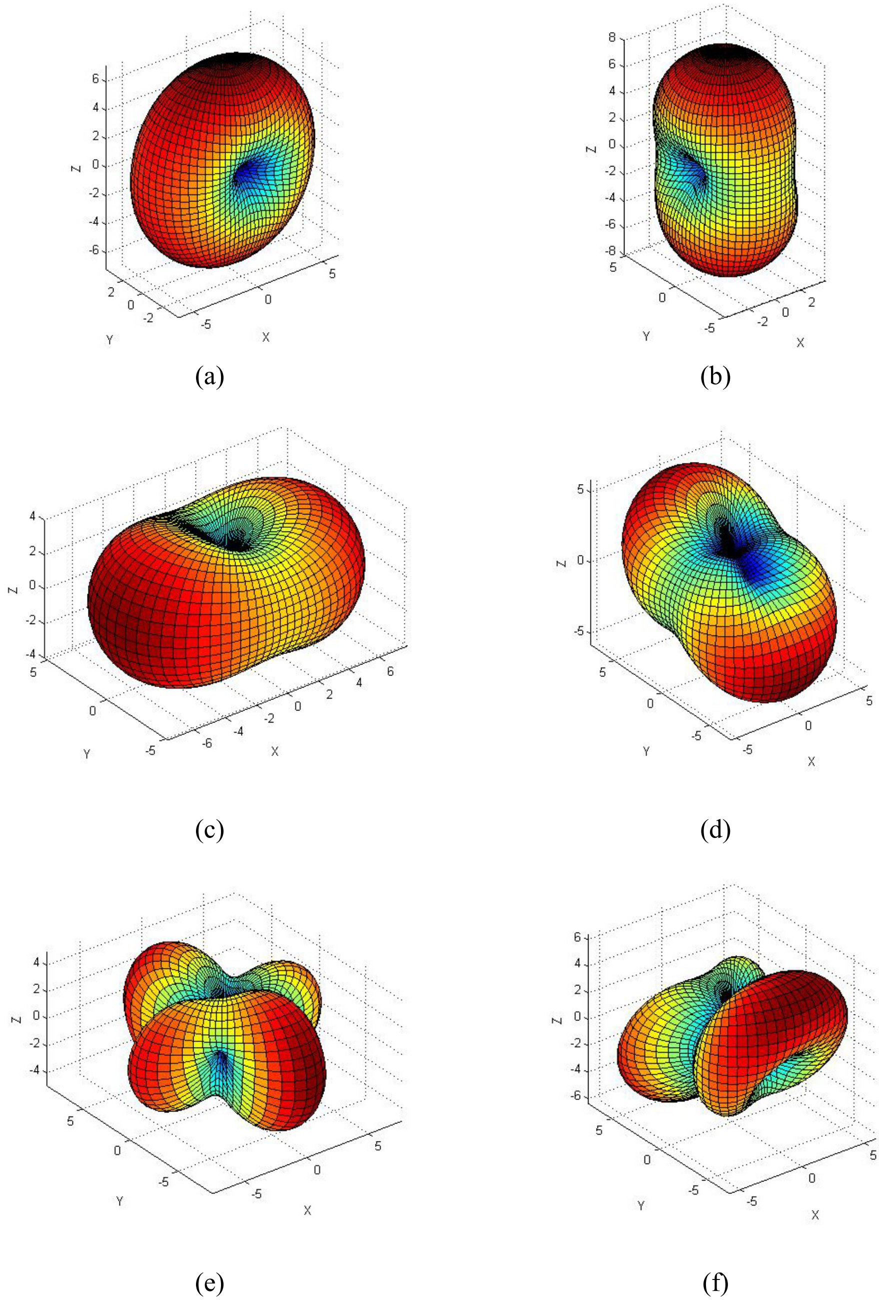

Figure 9.11: C-Fed prototype modal far-field patterns for (a) mode 1, (b) mode 2, (c) mode 3, (d) mode 4, (e) mode 5, and (f) mode 6

III. PIFA-monopole Prototype:

1. Current Distributions:

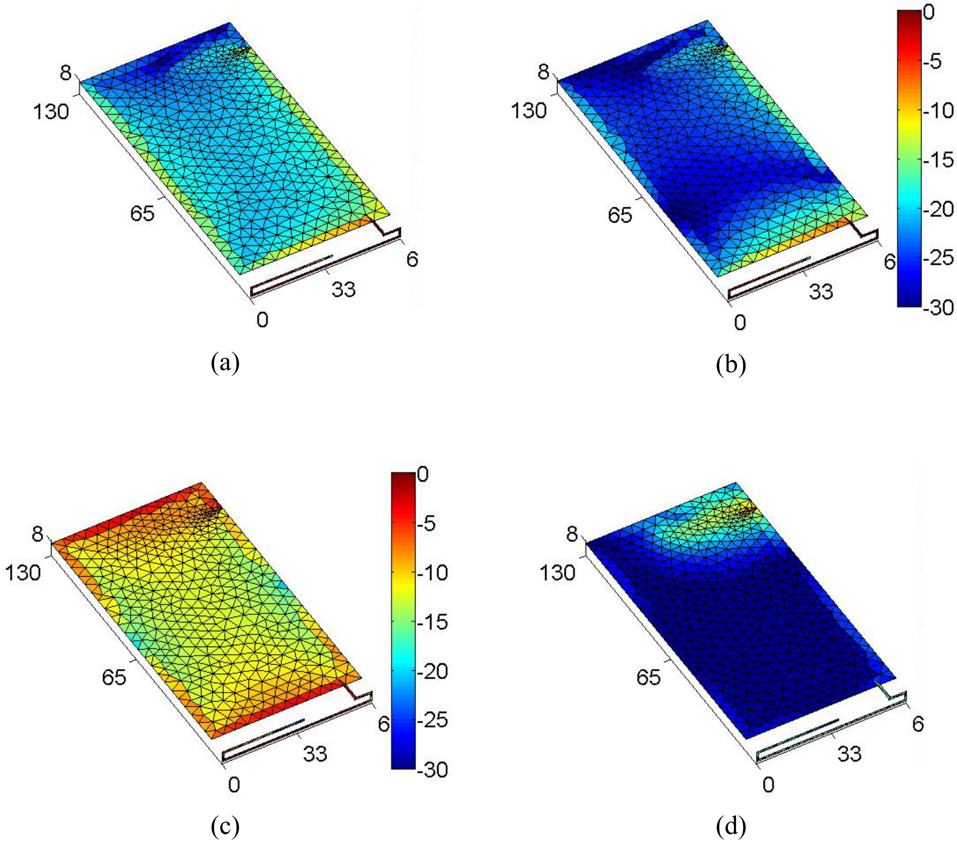

Figure 9.12: PIFA-monopole prototype modal current distributions for (a) mode 1, (b) mode 2, (c) mode 4, and (d) mode 5

2. Near-Fields:

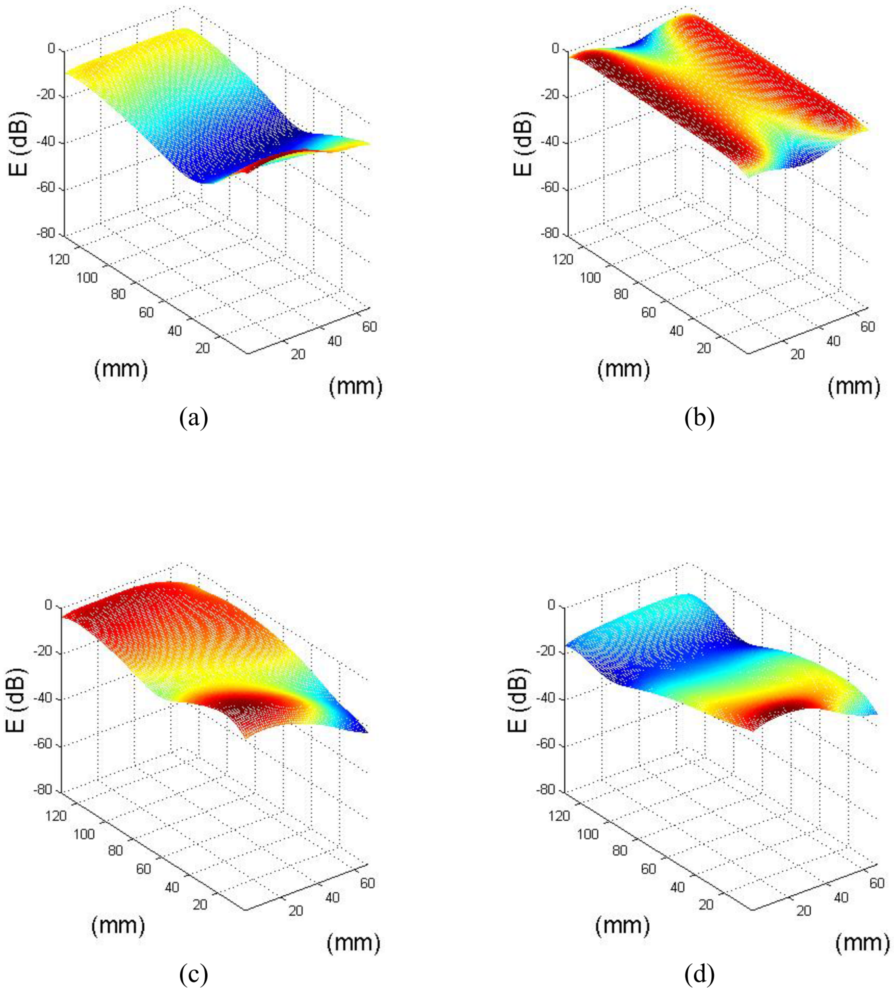

Figure 9.13: PIFA-monopole prototype modal electric near-fields for (a) mode 1, (b) mode 2, (c) mode 4, and (d) mode 5

3. Far-Fields:

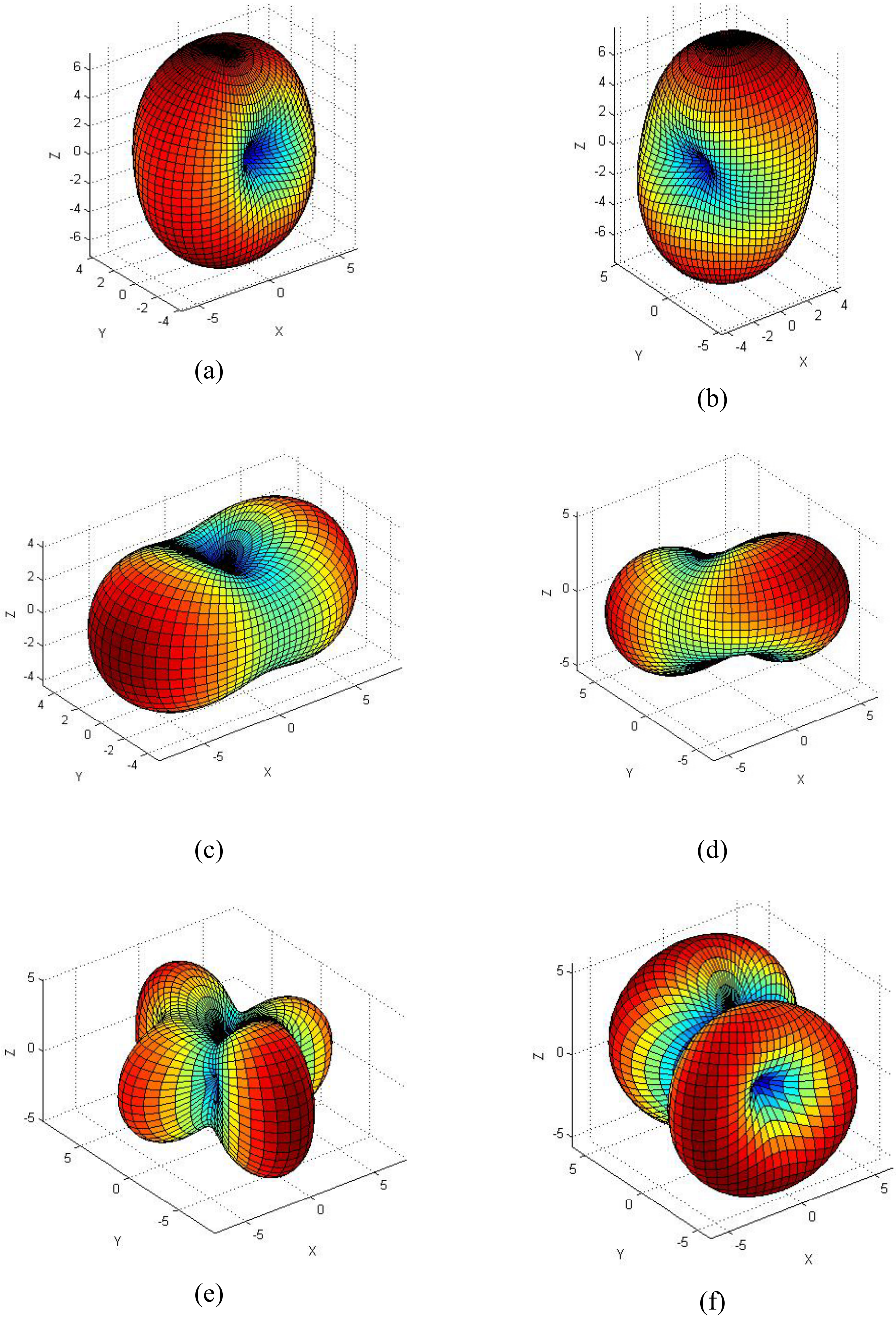

(a) (b) (c) (d) (e) (f)

Figure 9.14: PIFA-monopole prototype modal far-field patterns for (a) mode 1, (b) mode 2, (c) mode 3, (d) mode 4, (e) mode 5, and (f) mode 6

IV. T-strip Prototype:

1. Current Distributions:

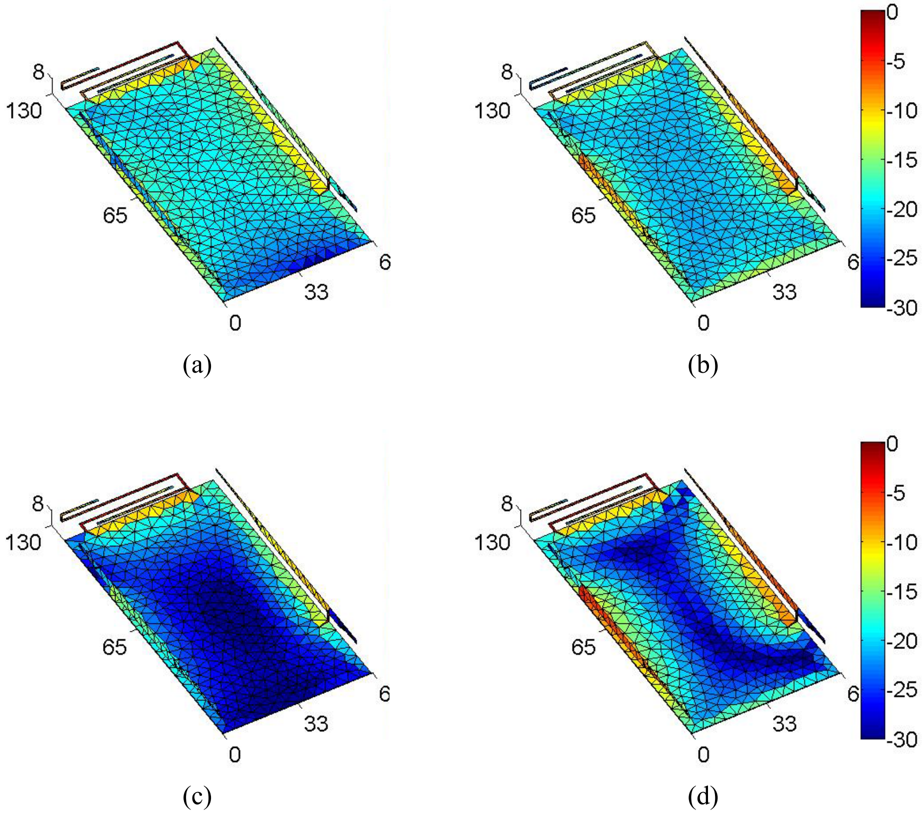

Figure 9.15: T-strip prototype modal current distributions for (a) mode 1, (b) mode 2, (c) mode 3, and (d) mode 4

2. *Near-Fields:*

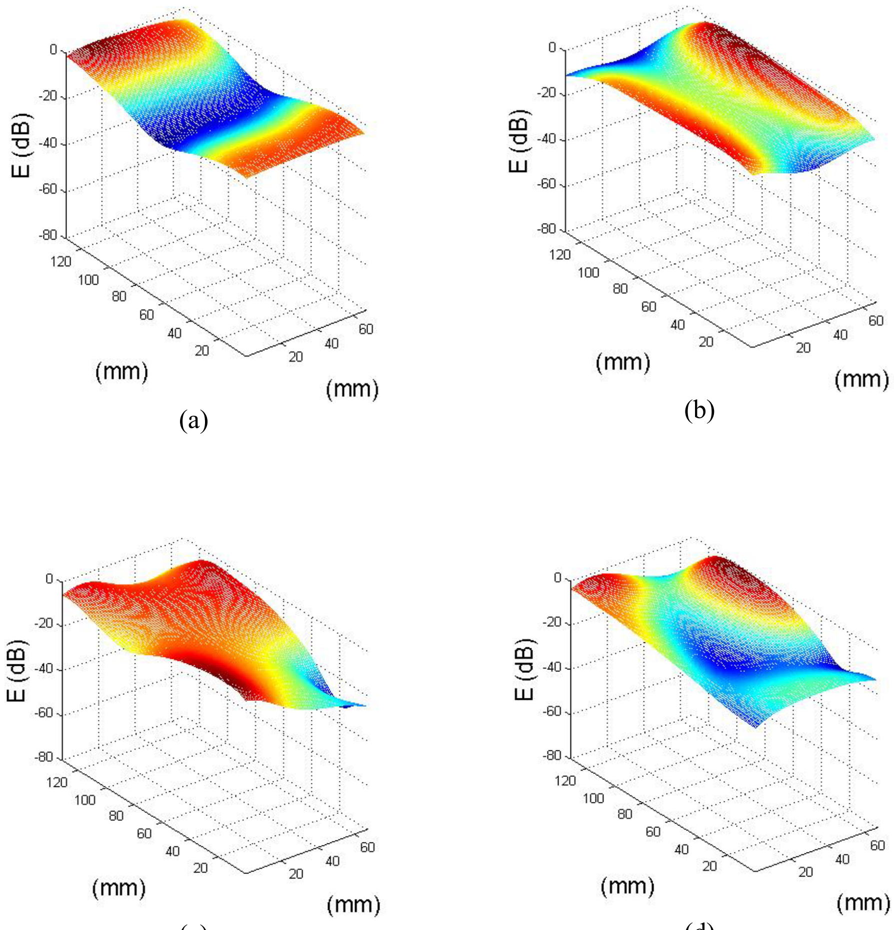

Figure 9.16: T-strip prototype modal electric near-fields for (a) mode 1, (b) mode 2, (c) mode 3, and (d) mode 4

3. Far-Fields:

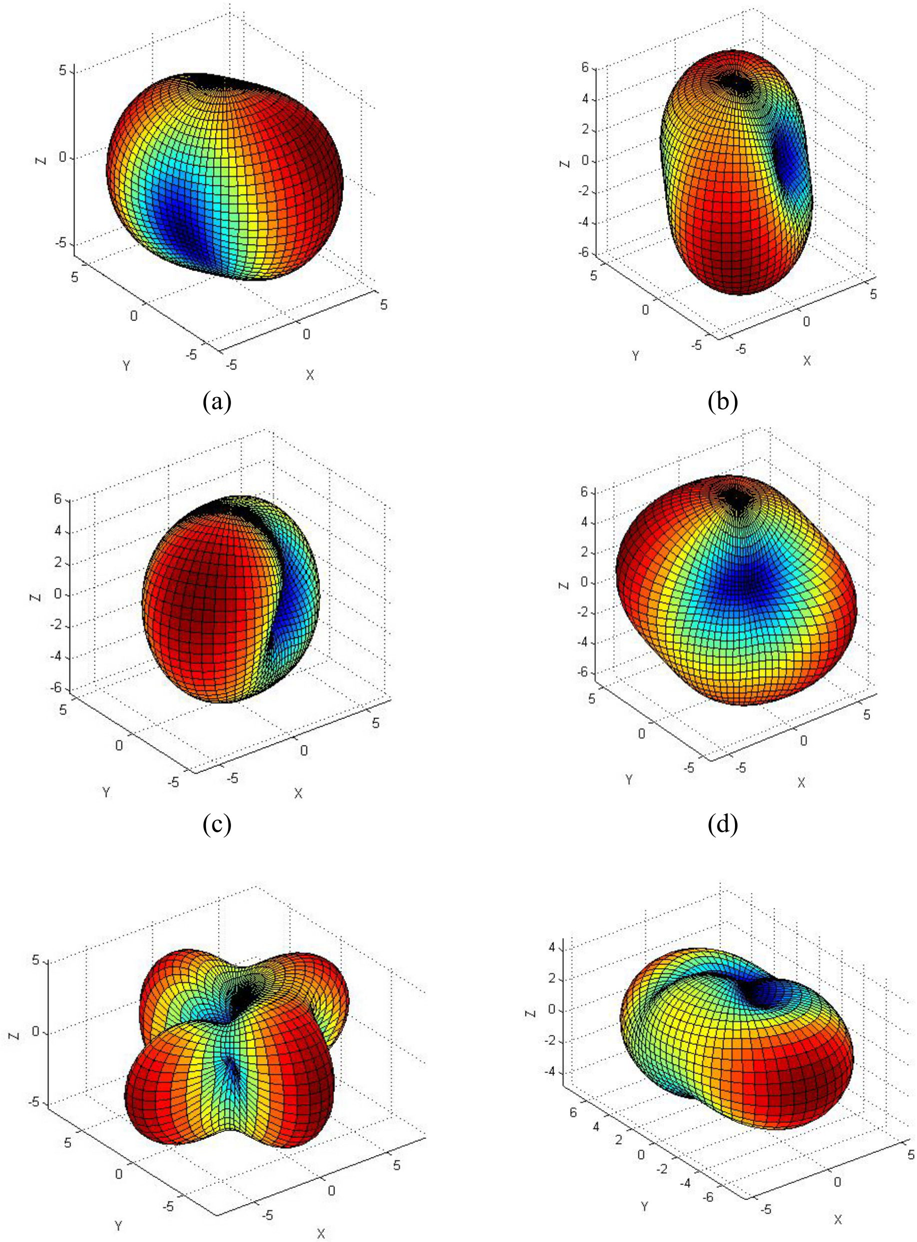

(a) (b)

(c) (d)

(e) (f)

Figure 9.17: T-strip prototype modal far-field patterns for (a) mode 1, (b) mode 2, (c) mode 3, (d) mode 4, (e) mode 5, and (f) mode 6

10 Bibliography

[1] Dahlman, E., Parkvall, S., and Sköld, J. (2012). *4G LTE-Advanced for Mobile Broadband.* Amsterdam: Academic Press.

[2] Lau, B. K. (2011). Multiple Antenna Terminals. In A. Sibille, C. Oestges, & A. Zanella, *MIMO From Thoery to Implementation*. San Diego: Academic Press, 267-296.

[3] Harrington, R. F., and Mautz, J. R. (1971). Theory of Characteristic Modes for Conducting Bodies. *IEEE Transactions on Antennas and Propagation,* 629-639.

[4] Garbacz, R. J., and Turpin, R. H. (1971). A Generalized Expansion for Radiated and Scaterred fields. *IEEE Transactions on Antennas and Propagation*, 348-358.

[5] Li, H., Tan, Y., Lau, B. K., Ying, Z., and He, S. (2012). Characteristic Mode Based Tradeoff Analysis of Antenna-Chassis Interactions for Multiple Antenna Terminals. *IEEE Transactions on Antennas and Propagation,* 490-502.

[6] Li, H., Lau, B. K., Ying, Z., and He, S. (2012). Decoupling of Multiple Antennas in Terminals With Chassis Excitation Using Polarization Diversity, Angle Diversity and Current Control. *IEEE Transactions on Antennas and Propagation,* 5947-5957.

[7] Li, H., Miers, Z., and Lau, B. K. (2013). Generating Multiple Characteristic Modes below 1GHz in Small Terminals for MIMO Antenna Design. *Antennas and Propagation Society International Symposium (APSURSI 2013)*, pp. 180 - 181.

[8] Li, H., Miers, M., and Lau, B. K. (2014). Design of Orthogonal MIMO Handset Antennas Based on the Characteristic Mode Manipulation at Frequency Bands below 1 GHz. *IEEE Transactions on Antennas and Propagation*, 2756-2766.

[9] Miers, Z., Li, H., and Lau., B. K. (2013). Design of Bandwidth-Enhanced and Multiband MIMO Antennas Using Characteristic Modes. *IEEE Antennas and Wireless Propagation Letters*, 1696-1699.

[10] Harrington, R. F., Mautz, J., and Chang, Y. (1972). Characteristic Modes for Dielectric and Magnetic Bodies. *IEEE Transactions on Antennas and Propagation,* 194-198.

[11] Garbacz, R. J. and Pozar, D. M. (1982). Antenna Shape Synthesis Using Characteristic Modes. *IEEE Transactions on Antennas and Propagation*, 340-350.

[12] Harrington, R. F., & Mautz, J. R. (1972). Control of Radar Scattering by Reactive Loading. *IEEE Transactions on Antennas and Propagation*, 446-454.

[13] Cabedo-Fabres, M., Antonino-Daviu, E., Valero-Nogueira, A., and Bataller, M. (2007). The Theory of Characteristic Modes Revisited: A Contribution to the Design of Antennas for Modern Applications. *IEEE Antennas and Propagation Magazine,* 52-68.

[14] Frank Demmerle, W. W. (2002). A Biconical Multibeam Antenna for Space-Division Multiple Access . *IEEE Transactions on Antennas and Propagation,* 782-787.

[15] Antonino-Daviu, E., Cabedo-Fabres, M., Gallo, M., Ferrando-Bataller, M., and Bozzetti, M. (2009). Design of a Multimode MIMO Antenna Using Characteristic Modes. *3rd European Conference on Antennas and Propagation (EuCAP 2009)*, 1840-1844.

[16] Solbach, K., and Famdie, C. (2007). Mutual Coupling and Chassis-Mode Coupling in Small Phased Array on a Small Ground Plane. *Second European Conference on Antennas and Propagation (EuCAP 2007),* 1-5.

[17] Rahola, J., and Ollikainen, J. (2006). Optimal Antenna Placement for Mobile Terminals Using Characteristic Mode Analysis. *First European Conference on Antennas and Propagation (EuCAP 2006)*, 1-6.

[18] Gallee, F., Bernabeu, T., Cabedo-Fabres, M., Daviu, E., and Nogueira, A. (2013). Application of the Theory of Characteristic Modes to the Design of Compact Metallic Strip Antenna with Multilayer Technology (LTCC). *7th European Conference on Antennas and Propagation (EuCAP 2013),* 1891-1895.

[19] Martens, R. C.-A., and Manteuffel, D. (2010). On the Relation between the Element Correlation of Antennas on Small Terminals and the Characteristic Modes of the Chassis. *Loughborough Antennas and Propagation Conference (LAPC 2010)*, 457-460.

[20] Martens, R., Safin, E., and Manteuffel, D. (2011). Inductive and Capacitive Excitation of the Characteristic Modes of Small Terminals. *Loughborough Antennas and Propagation Conference (LAPC 2011)*, 1-4.

[21] Lau, B. K., Andersen, J., Kristensson, G., and Molisch, A. (2006). Impact of Matching Network on Bandwidth of Compact Antenna Arrays. *IEEE Transactions on Antennas and Propagation,* 3225-3238.

[22] P. Vainikainen, J. Ollikainen, O. Kivekäs, and I. Kelander, Performance Analysis of Small Antennas Mounted on Mobile Handsets (2000). *COST 259 Final Workshop—The Mobile Terminal and Human Body Interaction*, 22.

[23] Martens, R., Safin, E., and Manteuffel, D. (2011). Selective Excitation of Characteristic Modes on Small Terminals. *5th European Conference on Antennas and Propagation (EuCAP 2011),* 2492-2496.

[24] Vainikainen, P., Ollikainen, J., Kivekas, O., and Kelander, I. (2003). Resonator-based Analysis of the Combination of Mobile Handset Antenna and Chassis. *IEEE Transactions on Antennas and Propagation,* 1433-1444.

[25] Best, S. R. (2009). The Significance of Ground-plane Size and Antenna Location in Establishing the Performance of Ground-plane-dependent Antennas. *IEEE Antennas and Propagation Magazine,* 29-43.

[26] Villanen, J., Ollikainen, J., Kivekas, O., and Vainikainen, P. (2006). Coupling Element Based Mobile Terminal Antenna Structures. *IEEE Transactions on Antennas and Propagation,* 2142-2153.

[27] Roshni, V. S., Revathy, K. (2008). Using Mutual Information and Cross Correlation as Metrics for Registration of Images. *Journal of Theoretical and Applied Information Technology* , 474-481.

[28] Cahill, N. D. (2010). Normalized Measures of Mutual Information with General Definitions of Entropy for Multimodal Image Registration. In B. M. Bernd Fischer (Ed.), *Biomedical Image Registration*. Lübeck: Springer Berlin Heidelberg, 258-268.

[29] Safin, E., and Mantueffel, D. (2013). Reconstruction of the Characteristic Modes on an Antenna Based on the Radiated Far Field. *IEEE Transactions on Antennas and Propagation*, 2964-2971.

[30] Plicanic, V., Vasilev, I., Tian, R., and B. K. Lau, B. K. (2011). On Capacity Maximisation of a Handheld MIMO Terminal with Adaptive Matching in an Indoor Environment. *IET Electronics Letters*, 900-901.

[31] Whiton, R., and Firouzabadi, F. (2012). Co-located Antenna Design in a Mobile Phone. *Master's Thesis*, Department of Electrical and Information Technology, Lund University.

[32] Plicanic, V., Lau, B. K., Derneryd, A., and Ying, Z. (2009). Actual Diversity Performance of a Multiband Antenna with Hand and Head Effects. *IEEE Transactions on Antennas and Propagation*, 1547-1556.

[33] Makarov, S. N. (2002). *Antenna and Electromagnetic Modelling with Matlab.* New York: John Wiley and Sons.

[34] Li, H., Lau, B., Tan, Y., and He, S. (2011). Impact of Current Localization on the Performance of Compact MIMO Antennas. *5th European Conference on Antennas and Propagation (EUCAP 2011)*, 2423-2426.

11 Related Materials

[35] *Dielectric Constant - Permittivity* . (2012). Retrieved 2014, from: http://maxwellsequations.com/materials/permittivity.php

[36] Company, Collins Radio. (1959). Chapter 10 Antenna Feed Systems. In C. R. Company, *Fundamentals of Single Side Band*, 1-20.

[37] Praveen Kumar, K. R. (2013). The Effect of Dielectric Permittivity on Radiation Characteristics of Co-axially Fed Rectangular Patch Antenna:

Design and Analysis. *International Journal of Advanced Research in Computer and Communication Engineering,* 1254-1258.

[38] Holopainen, J., Villanen, J., Icheln, C., and Vainikainen, P. (2006). Mobile Terminal Antennnas Implemented by Using Direct Coupling. *First European Conference on Antennas and Propagation (EuCAP 2006),* 1-6.

[39] Villanen, J., Ollikainen, J., Kivekas, O., and Vainikainen, P. (2003). Compact Antenna Structures for Mobile Handsets. *Vehicular Technology Conference*, 40-44.

[40] Capek, M., Hazdra. P., Hamouz, P., and Eichler, J. (2011). A Method for Tracking Characteristic Numbers and Vectors. *Progress in Electromagnetics Research B*, 115-134.

Series of Master's theses
Department of Electrical and Information Technology
LU/LTH-EIT 2014-418

http://www.eit.lth.se